Speleothem evidence of Late Glacial and Early Holocene Preboreal and Boreal hydro-climate change in western Mediterranean (Corchia Cave, Italy)

Andrea Columbu[1,2,*], Ilaria Isola[3], Giovanni Zanchetta[1,2,3], Russell N. Drysdale[4], Stefano Natali[1,5], John C. Hellstrom[4], Michel Magny [6], Anthony E. Fallick[7]

[1]Earth Sciences Department, University of Pisa, via S. Maria 53, 56126 Pisa, andrea.columbu@unipi.it giovanni.zanchetta@unipi.it

[2]CIRSEC-Centre for Climatic Change Impact, University of Pisa, Via del Borghetto 80, 56124 Pisa, Italy

[3]Istituto Nazionale di Geofisica e Vulcanologia, sez. di Pisa, Cesare Battisti 53, 56126 Pisa, Italy ilaria.isola@ingv.it

[4]School of Geography, Earth and Atmospheric Sciences, University of Melbourne, Victoria 3010, Australia rnd@unimelb.edu.au; john@ionium.net

[5]Institute of Geosciences and Earth Resources, IGG-CNR, via Moruzzi 1, 56124 Pisa, Italy stefano.natali@dst.unipi.it

[6]Chrono-Environment Laboratory, UMR 6249 CNRS-UFC, F-25030 Besancon cedex, France Michel.Magny@univ-fcomte.fr

[7]Scottish Universities Environmental Research Centre, East Kilbride G75 0QF, United Kingdom anthony.fallick@glasgow.ac.uk

*Correspondent author

Abstract

This paper explores the rainfall variability across the western Mediterranean area from ca. 12 to 9 ka, and its climate teleconnection within the Northern Hemisphere realm. A high-resolution stable isotope ($\delta^{18}O$, $\delta^{13}C$) and growth rate record from a Corchia Cave stalagmite (Apuan Alps, Central Italy) shows evidence of: 1) increased rainfall during the transition from the late Younger Dryas (YD) to the Holocene; and 2) two Early Holocene episodes of reduced rainfall during the so-called Preboreal and Boreal Oscillations (PBO and BO respectively). The YD to Holocene transition occurs at Corchia from $11.91^{+0.10}/_{-0.11}$ to $11.33^{+0.07}/_{-0.07}$ ka, in agreement with other Mediterranean records. The expression of PBO is constrained in Central Italy between $11.19^{+0.09}/_{-0.08}$ and $11.04^{+0.09}/_{-0.09}$ ka, while the BO from $10.42^{+0.13}/_{-0.27}$ to $10.19^{+0.27}/_{-0.24}$ ka, contemporaneous with a significant reduction of the Lago dell' Accesa lake levels (Central Italy).

The new record suggests that the increase of rainfall at Corchia during the deglaciation is connected to the enhanced evaporation from a warming North Atlantic and the higher moisture amount across the Mediterranean delivered by the westerlies. Reduced rainfall is instead attested during PBO/BOs. The latter are often associated with fluxes of ice-sheet meltwaters into the Atlantic, which trigger a deficit in moisture availability resulting in lower humidity reaching the Mediterranean area. This work confirms that the PBO/BO relative aridity is restricted to the Mediterranean area, while mid-European records point to moister conditions within the same events. Thus, our results imply that future – even subtle - polar ice sheet instabilities, boosted by the ongoing climate crisis, might amplify the change of rainfall dynamics across the western Mediterranean, a hot-spot area for climatic change that is already experiencing an increasing number of drought years.

Keywords: Holocene; Preboreal oscillation; Boreal Oscillation; deglacial; glacial termination; speleothem; lake level; Mediterranean

1. Introduction

The interval from the late last glacial to the Early Holocene Preboreal and Boreal intervals, occurring between ca. 12 and 9 kiloyears before 1950 CE (hereafter ka), testify to rapid climate changes of different amplitudes, characteristics and triggers (Buizert et al., 2014). During the last phase of the most recent deglaciation, global temperatures rose by around 3 ºC (Osman et al et al., 2021) in the well documented transition from the Younger Dryas (YD) to the Preboreal Holocene at ca. 11.65 ka (Rasmussen et al., 2014). At Arctic latitudes, this centennial increase may have reached 20 ºC (Buizert et al., 2018), concurrent with massive melting of residual icesheets, rises in CH_4 and sea level, and consequent reorganization of oceanic and atmospheric circulation (Skinner et al., 2010; Barker et al., 2011; Muschitiello et al., 2019; Dalton et al., 2020). Evidence of climatic deterioration during the very early Holocene has emerged from the North Atlantic region and across Central Europe, often referred to as the “Preboreal oscillation” (PBO) (Lotter et al., 1992; Björk et al., 1996, 1997; Hoek and Bos, 2007). In ice, terrestrial and marine chronologies, the earliest PBO is usually centred at around 11.2 ka, although the GICC05 Greenland ice chronology suggests the event occurred slightly earlier at ca 11.4 ka (e.g. Rasmussen et al., 2007). The origin of the PBO is unclear, possibly because of the difficulty in synchronising the different archives. Ice-sheet meltwater fluxes, changes in ocean ventilation and a decline in solar activity have been proposed as possible forcing

factors (e.g. Björk et al., 1997, 2001; Bond et al., 2001; Teller et al., 2002; van der Plicht et al., 2004; Magny et al., 2007). For example, Fisher et al. (2002) attributed the origin of this climate decline to a massive meltwater discharge event from glacial Lake Agassiz into the Arctic Ocean via the Mackenzie River. This flux started at 11.33 ka and lasted up until 10.75 ka, and may have decreased the formation of the North Atlantic Deep Water, reducing heat advection towards northern high latitudes. Another Early Holocene regional cooling, this time during the Boreal chronozone (e.g. Magny et al., 2001 and references therein), is the Boreal oscillation (BO), sharing similar triggers with the previous event and occurring around 10.3 ka (Hoek and Bos, 2007). Together, these PBO/BO events represent the earliest climate instabilities episodes among the suite that punctuated the Holocene, identified, for instance, by ice-rafted debris deposits (Bond et al., 2001).

Understanding how these global changes impacted local climate is pivotal for better comprehending the response of the lower latitudes to fluctuations in northern latitude boundary conditions. This is especially true in densely populated areas such as the Mediterranean, a global warming "hot-spot" (Giorgi, 2006) where past rainfall variations are clearly linked to high-latitude climate perturbations from ice-sheet melting (Garcia-Alix et al., 2021; Fohlmeister et al., 2023). The Italian mainland stretches north-south across the central and western Mediterranean area and in recent decades the country has been affected by severe rainfall extremes (e.g. Fink et al., 2003; Brunetti et al., 2004; Ionita et al., 2017), leading to important financial losses and causing several casualties. The study of the last deglaciation and the PBO/BOs allows understanding of the modality by which ice-sheet instabilities, of varied nature, extent and pace, affected the local climate. This has important implications for future climate modelling, as the ongoing Arctic warming will continue to alter rainfall patterns in the circum-Mediterranean area (IPCC, 2023). Higher instability of northern ice sheets is indeed expected for a warmer Holocene, as occurred during the warmer-than-present last interglacial (Tzedakis et al., 2018).

Italian – and thus central and western Mediterranean - past climate and environment variability has been intensely studied from terrestrial settings using different proxies (e.g. Allen et al., 1999; 2002; Magny et al., 2007; Zanchetta et al., 2022). In particular speleothems (cave calcite precipitates) have yielded important clues on hydro-climate variability during the Late Pleistocene and Holocene (e.g. Belli et al., 2013; Lechleitner et al., 2018; Regattieri et al., 2021; Columbu et al., 2024). A substantial contribution has been made by palaeoclimate records from Corchia Cave, through the study of $\delta^{18}O$-$\delta^{13}C$ and other geochemical characteristics that are mostly interpreted as hydrological indicators (Drysdale et al., 2020 and references therein). Conveniently, speleothems from Apuan Alps caves

have a high uranium content (Isola et al., 2019a), which provides precise U-Th dates upon which to construct reliable timeseries. Concurrently, the cave and surroundings have been monitored for several years (Piccini et al., 2008; Natali et al., 2021, 2022) in order to better understand how modern temperatures and rainfall dynamics imprint the chemistry of precipitation and cave drip-waters. Accordingly, the $\delta^{18}O$ of speleothems is a reliable proxy for rainfall amount and moisture source (Drysdale et al., 2009), while $\delta^{13}C$ is driven by the mode of hydrologically controlled dissolution processes as well as the vegetation activity in the catchment soils (Bajo et al., 2017).

Previous records from Corchia Cave did not cover in detail the late Glacial and early Holocene. This limits the possibility to further investigate this important period from a location where speleothem-derived proxies are well understood. This prevents a full understanding of the patterns of late glacial and early Holocene spatio-temporal climate variability for both the Italian region as well as the whole Mediterranean area, from where other records have been previously published (Badertscher et al., 2011; Grant et al., 2012; Siani et al, 2013; Toucanne et al., 2015; Bernal-Wormull et al., 2021; Surić et al., 2021; Columbu et al., 2022). In order to fill these gaps, this paper presents a decadally resolved speleothem record from Corchia Cave, spanning ca. 12 to 9 ka. The aim is to investigate the role of northern-latitude climate changes in driving late glacial and early Holocene hydro-climate variability in central-northern Italy, and their extent and propagation into neighbouring regions. As this cave lies in a mountainous climatically sensitive area, characterized by high annual precipitation influenced by Atlantic-sourced rainfall but also by Mediterranean cyclogenesis (i.e. from the Gulf of Genoa; Trigo et al., 2002), understanding the response of local hydroclimate to pre-industrial rapid global climate oscillations is considered key in light of current global warming.

2. Study area

Our data were obtained from stalagmite CC7, which was collected *in situ* from a deep chamber within Antro del Corchia (43° 59’ N, 10° 13’ E; Fig. 1), a cave formed in steeply dipping Mesozoic marbles and dolostones of the Apuan Alps (Isola et al., 2019a). The sampling site, *Galleria delle Stalattiti* (~835 m a.s.l.), is situated ca. 400 m below the surface and ca. 1 km from the nearest natural cave entrance (Drysdale et al., 2020). The chamber has a near-constant mean annual temperature of 8.4±0.3 ºC and receives its mean annual rainfall recharge of 2500-3000 mm over an elevation range of ca. 1200-1400 m (Piccini et al., 2008). Drip-waters in the chamber have a near constant oxygen isotopic composition ($\delta^{18}O_{drip}$: ca -7.4±0.3 ‰, Piccini et al., 2008), which is consistent with predicted values of rainfall at the estimated recharge elevation (Drysdale et al.,

2004; Piccini et al., 2008). Tritium data suggest that the percolation waters may have a mean residence time in the aquifer of ca. 50 years (Piccini et al., 2008). The surface above the cave is very steep and rugged, with large areas of bare karst rock. The sparse vegetation cover is confined to soil-filled solution features. Today the Apuan Alps climate has a predominantly North Atlantic influence, and recharge to the cave mainly originates from frontal systems arriving from the west (Fig. 1). Mediterranean storms also occur during summer. In the study area, a significant negative correlation exists between rainfall amount and the North Atlantic Oscillation index for the winter months (Natali et al., 2021; Luppichini et al., 2022).

3. Material and methods

CC7 is a ca. 20 cm long stalagmite (Fig. 1). The bottom half displays layering demonstrating at least six growth phases. For this study, CC7 was sampled at ca 200-µm resolution in the top half (ca. 7.6 cm) for $\delta^{18}O$ and $\delta^{13}C$, where the calcite appears as massive and translucent, with faint lamination. The bottom part is not considered in this study due to the complicated stratigraphy; unpublished ages indicate it developed discontinuously since at least 160 ka. The section of the stalagmite covering the last interglacial has been previously investigated (Drysdale et al., 2009; Tzedakis et al., 2018)

Stable isotope ($\delta^{18}O$ and $\delta^{13}C$) measurements were performed on ~0.75 mg powders using continuous-flow isotope-ratio mass spectrometry. Measurements were made on a GV Instruments GV2003 at the Advanced Mass Spectrometry Unit of The University of Newcastle (Australia), and on an Analytical Precision AP2003 at the Scottish Universities Environmental Research Centre (East Kilbride, UK). Samples were digested in 105 % phosphoric acid at 70°C and mass spectrometric measurements were made on the resulting CO_2 gas. Isotopic results are reported using the conventional δ notation in *per mille* (‰), and referred to the Vienna Pee Dee Belemnite scale (V-PDB) using the internal working standards of Carrara Marble (MAB1 – East Kilbride; NEW1 – Newcastle), which were calibrated against the international standards NBS18 and NBS19. Mean analytical precision for both $\delta^{18}O$ and $\delta^{13}C$ is better than 0.1 ‰. Replicate measurements were made where adjacent sample results differed by ≥0.4 ‰.

For U–Th dating, homogenised samples (n = 11) of up to 50 mg were extracted using a 0.7 mm drill bit. Subsamples were dissolved and spiked with a mixed $^{229}Th/^{233}U$ tracer before removal of the carbonate matrix using Eichrom TRU-Spec ion-exchange resin. The purified uranium and thorium fraction was introduced in dilute nitric acid to a Nu Instruments MC-ICP-MS, where $^{230}Th/^{238}U$ and

$^{234}U/^{238}U$ activity ratios were measured simultaneously using a parallel ion-counting procedure that allows for full internal standardization of ion-counter gain, elemental fractionation and mass bias. Full details of the analytical technique are provided in Hellstrom (2003; 2006) and updated in Drysdale et al. (2012). Ages were corrected for unsupported initial ^{230}Th on the basis of the measured $^{232}Th/^{238}U$ ratios and an assumed initial $^{230}Th/^{232}Th$ activity ratio of 0.8 ± 0.7, then calculated following Hellstrom (2003, 2006). The uncertainties on all ratios were fully propagated into the final ages (Table 1).

The $\delta^{13}C$ and $\delta^{18}O$ time series were tied to a Monte Carlo-derived age-depth model as described by Drysdale et al. (2005) (Fig.2). This model includes an uncertainty component that encompasses both sampling uncertainty introduced during the process of extracting powders for analysis, and age uncertainty arising from the corrected U–Th age determinations. Ages (in ka) refer to 1950 CE.

We applied a back-trajectory analysis to diagnose the origin and pathways of precipitating air masses at the study site, through the Hybrid Single-Particle Lagrangian Integrated Trajectory (HYSPLIT) model of the Air Resources Laboratory (ARL) of the National Oceanic and Atmospheric Administration (NOAA) (Stein et al., 2015; Rolph et al., 2017; Warner, 2018), with parameters of Natali et al. (2023). 5-day back trajectories were modelled every 6 hours at Corchia Cave each month from January 2021 to December 2021. 6 hours cumulative precipitation values were obtained using the hourly mean precipitation calculated by hourly rainfall records registered at the closest meteorological station of the Regional Hydrologic Service (SIR) (Terrinca - TOS02000064). Only trajectories corresponding to cumulative precipitation > 0 mm were selected, and with a relative integration error lower than 5%. A total of 508 5-day back trajectories were obtained from January to December 2021 (Fig. 1), indicating the westerly origin for most of the air masses with 6 hours cumulative rainfall > 0 mm at the study site.

4. Results

The U-Th ages have a low uncertainty (average 0.9 %, min 0.5 % max 1.6 %) due to a combination of the high uranium and low detrital thorium content (Table 1), the latter expressed by high values of $[^{230}Th/^{232}Th]_{activity}$. All ages are in stratigraphic order. According to the age model (Fig. 2), the portion of interest of CC7 was deposited between $11.93^{+0.10}/_{-0.11}$ and $9.46^{+0.32}/_{-1.92}$ ka. The average age-model uncertainty is +0.10 and -0.14 kiloyears (kyr). The growth rate is around 35 mm/kyr from the bottom to ca. 11.64 ka; here it doubles in less than two centuries, reaching the maximum values (ca. 75 mm/kyr) at 11.34 $^{+0.07}/_{-0.07}$ ka (Fig. 2). From here, there is an evident decrease to less than 30

mm/kyr centered at $11.11^{+0.09}/_{-0.11}$ ka. After a brief and moderate increase, the growth rate drastically decreases to less than 10 mm/kyr from $10.39^{+0.27}/_{-0.13}$ toward the top of the stalagmite. The mean temporal resolution of the resulting $\delta^{13}C$-$\delta^{18}O$ time series is ca. 7 years, ranging from 1 to 40 years.

The $\delta^{13}C$ and $\delta^{18}O$ range from -0.48 to 4.98 ‰ and from -5.27 to -2.47 ‰ respectively. Both $\delta^{13}C$ and $\delta^{18}O$ have their highest values within the first 1.2 mm of the bottom of the section, from $11.93^{+0.10}/_{-0.11}$ to $11.90^{+0.10}/_{-0.11}$ ka (Figs. 2 and 3). For the portion of CC7 younger than $11.90^{+0.10}/_{-0.11}$ ka, isotopic values are always significantly lower than the bottom part (Fig. 2). The presence of a short hiatus is suspected, separating these very high values from the rest of the dataset but this could not be resolved by U-Th dating (Fig. 2) and the age model, implying that the hiatus was shorter than 0.1 kyr (the average chronological uncertainty in the bottom part of the timeseries). The $\delta^{13}C$-$\delta^{18}O$ values after ~11.90 ka form two clusters: one with relatively higher isotopic ratios (from ~11.90 to ~11.33 ka), and the other with generally lower ratios (from 11.39 ka to ~9.46) (Fig. 3). From ~11.90 ka, the $\delta^{18}O$ shows a trend toward the lowest value of -5.27 ‰ that is reached at $10.64^{+0.13}/_{-0.09}$ ka, but is interrupted by short reversals, the most pronounced of which are centred at $11.68^{+0.09}/_{-0.10}$, $11.49^{+0.09}/_{-0.09}$, $11.36^{+0.07}/_{-0.07}$ and especially $11.11^{+0.09}/_{-0.11}$ ka (Fig. 2). This latter documents a reduction of ca. 0.4 ‰ lasting for ca. 150 years from $11.19^{+0.09}/_{-0.08}$ to $11.04^{+0.09}/_{-0.09}$ ka. From ~10.65 ka there is another prominent ca. 0.7‰ increase of $\delta^{18}O$ values with two peaks at $10.39^{+0.27}/_{-0.13}$ and $10.28^{+0.27}/_{-0.20}$ ka. From the latter age point to the top, there is a final trend towards lower values, with two sudden increases centred at $9.91^{+0.25}/_{-0.19}$ and $9.73^{+0.81}/_{-0.23}$ ka that create a seesaw pattern. The $\delta^{13}C$ record shares some similarities with $\delta^{18}O$, especially in the general decreasing trend occurring in the older part (Fig. 2). In this case, the trend ends at $10.90^{+0.08}/_{-0.06}$ ka and it is interrupted by the most rapid shift toward lower $\delta^{13}C$ values at $11.68^{+0.09}/_{-0.10}$ ka, creating a ca. 150 years duration period where some of the lowest values of the entire dataset occur. Reversals toward higher values are almost coincident with those in $\delta^{18}O$, and centred at $11.70^{+0.10}/_{-0.10}$, $11.54^{+0.10}/_{-0.09}$, $11.31^{+0.07}/_{-0.07}$ and $11.10^{+0.09}/_{-0.11}$ ka. The latter is a century-long increase from $11.22^{+0.08}/_{-0.09}$ to $11.07^{+0.09}/_{-0.09}$ ka. After ~10.90 ka, throughout the younger part of the speleothem and until the top, there are several other oscillations toward higher (centred at $10.57^{+0.10}/_{-0.19}$, from $10.39^{+0.13}/_{-0.27}$ to $10.17^{+0.27}/_{-0.22}$, and $9.91^{+0.19}/_{-0.25}$ ka) and lower (centred at $10.45^{+0.13}/_{-0.25}$, $9.99^{+0.17}/_{-0.23}$ and $9.84^{+0.18}/_{-0.23}$ ka) values and a sudden increase of $\delta^{13}C$ toward the topmost section.

5. Discussion

5.1. Replication of CC7 record

The $\delta^{18}O$-$\delta^{13}C$ from speleothems can provide reliable climate and environmental information if calcite is deposited under quasi-equilibrium conditions, which implies that "random" isotopic values given by kinetic fractionation does not play a dominant role. The Hendy test has been largely used in speleothem science to ascertain equilibrium vs non-equilibrium conditions (Hendy, 1971), although today it is not considered as definitive proof (Dorale and Liu 2009; Mühlinghaus et al., 2009; Day and Henderson, 2011). The "replication test" is instead considered a better approach (Dorale and Liu 2009). It consists of comparing coeval $\delta^{18}O$ timeseries from speleothems from the same cave. If they substantially agree, significant kinetic effects can be excluded, or at least assumed not to dominate the isotope signals. Stalagmite CC26 was retrieved from the same cave chamber as CC7 (Zanchetta et al., 2007). The original CC26 age model (Zanchetta et al., 2007) was updated by Bajo et al. (2017) based on a larger set of U/Th ages. We use the CC26 $\delta^{18}O$ time series as a replication test for CC7.

By considering the original $\delta^{18}O$ timeseries, CC7 and CC26 demonstrate high degree of similarity, along with some discrepancies. Starting from these latter, the decreasing $\delta^{18}O$ trend characterising CC7 from ~11.90 to ~10.64 ka is less pronounced in CC26 (Fig. 4a). While the absolute values and trend coincide up to ~11.35 ka, from this point onward the CC26 values plateau. Accordingly, this results in average $\delta^{18}O$ values that are up to 0.5‰ higher in CC26 with respect to CC7. However, we are aware that different altitudes of recharge feeding the two stalagmites can induce isotopic variations in coeval stalagmites, as suggested by Tzedakis et al. (2018) for the part of CC7 deposited during the last interglacial. Indeed, the cave chamber where CC7 and CC26 have been retrieved lies 400 m below the surface and receives rainfall recharge over an altitudinal range of ca. 1200-1400 m. In the Apuan Alps, an average $\delta^{18}O$/altitude rainfall gradient of -0.15‰/100 m has been determined (Natali et al., 2022), meaning that the $\delta^{18}O$ composition of seepage feeding the stalagmites can be enriched/depleted up to 0.30‰. This average gradient is obtained by linear interpolation (Natali et al., 2022), although the $\delta^{18}O$/altitude relationship could be here non-linear due to the exacerbation of Raleigh fractionation as T decreases with altitude, eventually producing an even higher gradient (Tzedakis et al., 2018). Additionally, coeval records from the same cave frequently display differences in mean, variability and trends (Treble et al., 2022), because the individual stalagmites are fed by individual flowpaths with different isotopic composition. By an analysis of 146 globally distributed coeval pairs of speleothems, it has indeed demonstrated that the within-cave speleothem $\delta^{18}O$ variability is 0.4‰, with 51 caves exceeding this value (Treble et

al., 2022). 0.5‰ is instead the within-cave variability of dripwater, analysing the data from 50 caves (Treble et al., 2022). Overall, the interplay of recharge at different altitude and the peculiar isotopic composition of individual flowpaths feeding CC7 and CC26 explain the ca. 0.5‰ difference in average $\delta^{18}O$ values from ~11.45 to ~9.5 ka, as well as that some short range isotopic variability appears as smoothed, muted and/or more pronounced in one stalagmite and *vice versa*. The different chronological resolution of the two timeseries plays also a role in smoothing the signal.

Apart from this 0.5‰ discrepancy, the $\delta^{18}O$ of CC7 and CC26 shows a good visual agreement (Fig. 4). To better investigate the replicability of the two records, we apply the intra-site correlation age modelling (iscam) approach (Fohlmeister 2012a) by using the parameters suggested by the author. The results show that the two $\delta^{18}O$ timeseries are strongly correlated (r=0.87) within the overlapping period. Iscam also includes a detrending module (Fig. 4b) by which to construct a composite record (Fig. 4c). The detrended timeseries are coincident in terms of shape and absolute values, although the correlation is reduced (r=0.67). The major climate events that are the focus of this work appear in both the original and detrended curves. Accordingly, the composite record shows the same characteristics. Such agreement points to the exclusion of predominantly kinetic deposition. However, it brings into question which is the best record for further climate interpretation between CC7, CC26 or the iscam-composite. We select CC7 because its average growth rate of 37 mm/kyr, is more than twice that of CC26 (14 mm/kyr, Zanchetta et al., 2007; Bajo et al., 2017), giving It an average resolution of ca. 7 years compared to ca. 20 years for CC26.

5.2. Interpretation of CC7 $\delta^{18}O$-$\delta^{13}C$

There is a wealth of evidence that $\delta^{18}O$ in Corchia speleothems captures changes in rainfall amount effect from multimillennial to centennial timescales (Bajo et al., 2020 and references therein), except during intervals of significant North Atlantic ocean source-water $\delta^{18}O$ changes such as during Termination II (Tzedakis et al. 2018; Drysdale et al. 2020). Accordingly, $\delta^{18}O$ values decrease during wetter periods and increase during drier ones. In speleothems, the amount effect predominates around the central and western Mediterranean region (Columbu et al., 2020) because the temperature-controlled isotopic fractionation during calcite precipitation (estimated between -0.18°C/‰ (Tremaine et al., 2011) and -0.24°C/‰ (Kim and O'Neil, 1997), averaging -0.21°C/‰) almost equals the air temperature effect on rainfall, which is ca. +0.2 °C/‰ in Tuscany (Natali et al., 2021). On average, this cancels the temperature-driven effect of the isotopic fractionation between calcite and water (Piccini et al., 2008). A recent study on Pianosa Island, ca. 150 km south of Corchia,

290 demonstrates that moisture source has a net impact on current rainfall isotopic composition, at
291 times higher than rainfall amount (Natali et al., 2023). Here, the majority of the moisture is received
292 from intra-Mediterranean locations, generating rainfall $\delta^{18}O$ higher than extra-Mediterranean (i.e.
293 especially Atlantic) sourced moisture. Pianosa and Corchia sites are not directly comparable; the
294 first is a small low-relief, low-altitude landmass, with an average annual temperature and rainfall of
295 16.5 ºC and 567 mm respectively, characterised by an arid summer. The Corchia area is on the other
296 hand mountainous, annual average temperatures are lower (ca. 8 ºC) and rainfall is from 5 to 6
297 times more abundant than Pianosa, with no arid season (Natali et al., 2022). Most importantly, the
298 high-elevation Apuan Alps provide a topographic barrier for the westerly-sourced humidity,
299 intercepting the arrival of the Atlantic frontal systems and at times producing intense meteoric
300 events. The reconstruction of back trajectories (Fig. 1) clearly indicates the westerly origin
301 throughout the year for most of the air masses with 6 hours cumulative rainfall > 0 mm. Many such
302 events by-pass or do not impinge upon the rainfall at Pianosa, leaving this island mostly subjected
303 to intra-Mediterranean sourced rainfall. However, it is possible that during periods of lower
304 evaporation of the Atlantic, such as during glacials or stadials, in Corchia the ratio of
305 Atlantic/Mediterranean sourced rainfall was lower than during interglacials or interstadials
306 (Drysdale et al., 2009), with Atlantic-sourced rainfall $\delta^{18}O$ being lower than that which is
307 Mediterranean-sourced (e.g. Celle-Jeanton et al., 2004; Longinelli et al., 2006). Accordingly,
308 moisture source has also been considered as influencing Mediterranean speleothem $\delta^{18}O$,
309 especially during glacial to interglacial transitions (Columbu et al., 2022) or within the last glacial's
310 most prominent climate oscillations (Columbu et al., 2020). Thus, we interpret the CC7 $\delta^{18}O$ to be a
311 palaeohydrological indicator mostly driven by rainfall amount, with rainfall source changes having
312 a secondary effect in modulating the final speleothem isotopic signature.
313 The interpretation of $\delta^{13}C$ in speleothems is less straightforward than for $\delta^{18}O$ (Fohlmeister et al.,
314 2020), which explains why the former is usually used to support the interpretation of the latter,
315 rather than used as an independent proxy. A detailed study of $\delta^{13}C$ in Corchia speleothems (Bajo et
316 al., 2017) further highlights the complicated interplay of processes determining the final values in
317 this study area: i) open- vs closed-system bedrock dissolution; ii) sulphuric vs carbonic acid bedrock
318 dissolution; iii) CO_2 from both soils and old organic matter; and iv) prior calcite precipitation (PCP).
319 Accordingly, the very high $\delta^{13}C$ values in CC7 (up to 5.0‰, but the overwhelming majority of values
320 between 0.0 and 1.0 ‰) agree with carbon prevalently sourced from the bedrock (at times,
321 sulphuric-acid-dissolution derived) rather than from biogenic CO_2 from soils (Bajo et al., 2017),

which otherwise produces speleothem $\delta^{13}C$ values considerably lower than 0‰ (McDermott, 2004). However, the abovementioned interplays can drive the final speleothem $\delta^{13}C$ values in the same direction because periods of lower vs higher rainfall impact the water residence time and thus the modality of carbon uptake and release by the infiltrating groundwaters. We follow the interpretations of Bajo et al. (2017), who related higher (lower) $\delta^{13}C$ as due to a general reduction (increase) of hydrogeological circulation due to lower (higher) rainfall. Importantly, this process is more prominent during glacial-to-interglacial transitions, where also higher $\delta^{13}C$ values indicate a low contribution from biogenic CO_2, and *vice versa.* Oppositely, climate shifts of minor intensity might not produce the same effect.

5.3. Late Glacial to Holocene transition from stalagmite CC7

The highest values of both $\delta^{18}O$ and $\delta^{13}C$ from $11.93^{+0.10}/_{-0.11}$ to $11.91^{+0.10}/_{-0.11}$ ka (Figs. 2 and 3) record the late glacial phases of lowest rainfall amount at Corchia. Within age uncertainties, this is chronologically in agreement with a minimum in rainfall in southern Italy at $12.10^{+0.15}/_{-0.14}$ ka (Columbu et al., 2022) as well as a maximum of planktic foraminiferal $\delta^{18}O$ from the Iberian Atlantic margin at $11.69^{+0.30}/_{-0.30}$ ka (Hodell et al., 2013) (Fig. 5). At the same time, Mediterranean pollen in Monticchio is below 50% (Allen et al., 2002) pointing to climate deterioration in southern Italy, and there are low sea-surface temperatures (SST) in the Adriatic Sea (Siani et al., 2013) and low continental temperatures in northern Spain (Bernal-Wormull et al., 2021) and central Europe (von Grafenstein et al., 1999) (Fig. 6). This period fits with the last phase of Greenland stadial 1 (NGRIP, 2004), within the late Younger Dryas (YD) chronozone, when Greenland experienced the most recent temperature minimum prior to the Holocene (Fig. 6).

The YD expansion of Northern Hemisphere ice-sheets had a role in reducing the availability of moisture because of the decline in temperatures and related minor evaporation from the Atlantic (Drysdale et al., 2009; Columbu et al., 2022) consequently causing the most arid period recorded by CC7 during the terminal part of the YD. With less moisture contribution from the Atlantic, this was likely the time when the Mediterranean was the main source of moisture for rainfall at the Corchia site. The reduced ratio of Atlantic/Mediterranean-sourced rainfall thus contributed to the highest $\delta^{18}O$ values.

The progressive CC7 $\delta^{18}O$ lowering between $11.91^{+0.10}/_{-0.11}$ to $11.33^{+0.07}/_{-0.07}$, interpreted as an increase of rainfall, marks the YD-Holocene transition at Corchia (Fig. 5). The CC7 $\delta^{13}C$ does not show a comparable progressive trend as does $\delta^{18}O$, but a rapid shift is visible at $11.68^{+0.09}/_{-0.10}$ ka (Fig. 2).

Instead, growth rate in CC7 doubles from ~11.65 to ~11.45 ka, and this shift is centred at $11.54^{+0.10}/_{-0.09}$ ka (Fig. 2). The rapid increase of rainfall that, in southern Italy (Columbu et al., 2022), has been attributed to the last step of the YD-Holocene transition, occurs at $11.95^{+0.15}/_{-0.19}$ (Fig. 5); in Greenland, the end of the YD coincides with a large shift towards higher temperatures at $11.65^{+0.10}/_{-0.10}$ ka (Fig. 6). In the Corchia karst system, water residence time is around 50 years (Piccini et al., 2008) and, above the *Galleria delle Stalattiti*, the caprock is thick at ca. 400 m. For these reasons, the $\delta^{18}O$-$\delta^{13}C$ climate-driven signal might present a more delayed response with respect to the changes occurring at the surface (Zanchetta et al., 2007), considering the size of plumbing systems. However, fast growth rate depends on the combined effect of increasing drip-rate and higher dissolved $CaCO_3$ in the infiltrating waters. These are the most suitable conditions for calcite precipitation at around $11.54^{+0.10}/_{-0.09}$ ka, and this age is attributed to the establishment of interglacial conditions at our study site.

In the Northern Hemisphere, the rapid temperature rise during the last deglacial caused the retreat of northern ice-sheets and consequent atmospheric and oceanic reorganization (Skinner et al., 2010; Muschitiello et al., 2019; Dalton et al., 2020). This is the time of higher availability of Atlantic moisture, producing higher rainfall at the Corchia site, simultaneously with the rise of temperature in Continental Europe as well as in the circum-Mediterranean area (Fig. 6). Opposite to the YD conditions, the Atlantic/Mediterranean-rainfall sourced ratio was higher, contributing to decreasing $\delta^{18}O$ in CC7. Interestingly, the decrease of $\delta^{18}O$ (ca. 1.2‰) in the Iberian margin planktic foraminifera throughout the transition toward the Holocene, from ~11.6 to ~10.6 ka, is similar to that in CC7 (Fig. 5). The two records differ by up to 400 years during the phase of the most rapid isotopic decrease, likely due to the inferior age control in the ocean record. However, the lowest values of planktic $\delta^{18}O$ reached at around 10.65 ka are in perfect agreement with the lowest values of CC7 $\delta^{18}O$ at $10.64^{+0.13}/_{-0.09}$ ka (Fig. 5). This possibly marks the wettest period recorded by CC7, when the Atlantic/Mediterranean-rainfall sourced ratio was at its maximum. As deglacial planktic $\delta^{18}O$ is sensitive to the combined effect of water temperature increase and the supply of isotopically light oxygen from the melting ice sheets (Hodell et al., 2013), the change of the isotopic composition of the moisture source is here potentially enhancing the CC7 $\delta^{18}O$ trend.

5.4. Preboreal and Boreal climate oscillations

Climate instabilities have been identified from 11.4 to 11.1 ka and from 10.4 to 10.2 ka (Björk et al., 1996, 1997, 2001) in lacustrine and glacial records from northwest Europe, respectively in preboreal

and boreal times, and referred as PBO and BO. From northern hemisphere high latitude to central Europe there is a general agreement for this chronology (Lotter et al., 1992; Björk et al., 1996, 1997; Magny and Begeot 2004; Hoek and Bos, 2007; 2001; Teller et al 2002; Fiłoc et al., 2018), with PBO/BO being associated with general colder conditions and variable rainfall according to the latitude as well as local peculiarities. For example, a compilation of lake level (fig. 7) records suggests wetter conditions in west-central Europe while drying is detected in north-central Italy (Magny et al., 2007), although the dataset is biased toward the central-Europe location. CC7 $\delta^{18}O$ exhibits two prominent excursions during the early Holocene: one between $11.19^{+0.09}/_{-0.08}$ to $11.04^{+0.09}/_{-0.09}$ ka and thus centred at $11.11^{+0.09}/_{-0.11}$ and another from $10.42^{+0.13}/_{-0.27}$ to $10.19^{+0.27}/_{-0.24}$ ka and thus centered at $10.28^{+0.27}/_{-0.20}$ ka (Figs. 2 and 6). These are replicated in CC26 (fig. 4) and are coupled with a substantial reduction of CC7 growth rates (Fig. 2). The increase in CC7 $\delta^{18}O$ during the Holocene, when deglaciation is completed, would fully mirror a reduction of rainfall amount as explained above. Their occurrence within the timeframe proposed for PBO and BO (Björk et al., 1996, 1997, 2001), and the presence of similar intervals of climate deterioration in nearby records (Fig. 6), suggests they are the local expression of the PBO and BO in the western Mediterranean. For simplicity, we refer to the events centred at $11.11^{+0.09}/_{-0.11}$ ka and $10.28^{+0.27}/_{-0.20}$ ka as PBO-11.1 and BO-10.3 respectively when considering CC7 record.

The correlation with Lago dell' Accesa, ca. 150 km south of Corchia (Magny et al., 2007; Fig. 7 and 8), is particularly instructive to: 1) assess the reliability of CC7 $\delta^{18}O$ record as paleorainfall indicator; and 2) sustain the regional significance of PBO/BO dryness in northern-central Italy previously suspected (Magny et al., 2007). Lago dell' Accesa is a sink-hole lake fed by a spring and local rainfall, making it particularly suitable for the investigation of lake-level variability through time. Lake level was reconstructed using a comprehensive stratigraphic approach and supported by the study of lacustrine carbonate concretions (Magny et al., 2007). Lake-level reconstructions suggest that the PBO/BOs are: i) synchronous in the two records (within the age errors of both successions, i.e. within 1 century for the onset, peak and demise of the climate oscillations); and ii) marked by a lowering of the lake level, consistent with a reduction in runoff to the lake, corroborating the interpretation of the CC7 $\delta^{18}O$ as a rainfall amount proxy. PBO-11.1 is the shorter and more abrupt, lasting for ca. 150 years. According to the CC7 chronology, it spans $11.19^{+0.09}/_{-0.08}$ to $11.04^{+0.09}/_{-0.09}$ ka and an increase of ca. 0.4‰ of CC7 $\delta^{18}O$ is correlated to a drop of around 2.5 m of the Lago dell'Accesa lake level (Fig. 7). From $10.64^{+0.13}/_{-0.09}$ to $9.99^{+0.17}/_{-0.23}$ ka the agreement between the CC7 $\delta^{18}O$ and Lago dell'Accesa records is impressive, and an increase of ca. 0.7‰ of the first is correlated with a total

418 drop of the second of ca. 2.8 m. PBO-10.3 is here defined in the peak of this u-shaped trend from
419 $10.42^{+0.13}/_{-0.27}$ to $10.19^{+0.27}/_{-0.24}$ ka, when lake level reaches the minimal and CC7 $\delta^{18}O$ the maximal
420 values. In Lago dell'Accesa, charcoal analyses show increased fire frequency during the low lake level
421 of the PBO/BOs, suggesting that fires were promoted by drier conditions, probably driven by drier
422 summers (Vanniere et al., 2008). Furthermore, even the main shifts toward lower CC7 $\delta^{18}O$ values
423 that mirror an increase in precipitation are aligned with similar trends of higher lake levels at Lago
424 dell'Accesa, indicating that the two systems are responding to the same climate trigger.
425 Contrary to $\delta^{18}O$, a weaker correlation exists between the lake level and CC7 $\delta^{13}C$ (Fig. 7). The two
426 records mostly agree during BO-10.3 and, interestingly, during the first phases of the deglaciation
427 at around 11.65 ka. This is a further indication that the response of $\delta^{13}C$ at Corchia site is more
428 pronounced during marked changes in hydro-climate, while episodes of minor magnitude might not
429 be recorded and/or they are masked by the effects of processes unrelated to climate and/or long-
430 term soil development in the Corchia recharge area.
431 To our knowledge, *ad hoc* studies aimed to investigate PBO/BO by using speleothems are virtually
432 absent. We anyway noticed that evidence of PBO-11.1 and especially BO-10.3 (Fig. 6 and 8) is
433 traceable in speleothems from Sant'Angelo Cave southern Italy (Columbu et al 2022), coherently
434 recording lower rainfall. Although of very low resolution, pollen data from Monticchio Lake in
435 Southern Italy (Fig. 6) is in agreement at least for PBO-11.1. Speleothems from northern Spain that,
436 instead, represent temperature variation point to moderate cooling during PBO-11.1 (Fig. 6 and 8),
437 while a more robust decrease is evident earlier, at ca. 11.4 ka. Temperature-dependent ostracods
438 $\delta^{18}O$ from Ammersee Lake (central Germany)(von Grafenstein et al., 1999) and quantitative
439 temperature reconstructions from speleothem fluid inclusions from Milandre Cave (northwestern
440 Switzerland) (Affolter et al., 2019) (Fig. 6), also detect a more pronounced cooling at 11.4 ka rather
441 than at 11.1 ka. This is also evident in Greenland $\delta^{18}O$ (NGRIP, 2007). The Greenland and central
442 European records reported above seems instead insensitive at BO-10.3 (Fig. 6 and 8), although a
443 possible cold spell is visible at ca. 10.3 ka in Bunker Cave $\delta^{18}O$ in central Germany (Fohlmeister et
444 al., 2012b), which unfortunately does not extend over 11 ka to address PBO-11.1 too. Indeed, a
445 recent speleothem $\delta^{18}O$ time series from Blessberg Cave in central Germany (Breitenbach et al.,
446 2019) points to moderate climate deterioration centred at ca. 11.4 ka, although climate is not
447 varying substantially around 10.3 ka.
448 Interestingly, two additional PBOs appear to be preserved in CC7 at $11.48^{+0.09}/_{-0.08}$ and $11.36^{+0.07}/_{-}$
449 $_{0.07}$ ka, where $\delta^{18}O$ shows rapid changes of about 0.5 ‰ toward higher values. These presumed

450 “PBO-11.5” and “PBO-11.4” can be detected in Mediterranean archives (Fig. 6), including close
451 synchronicity with the Lago dell’Accesa (Fig. 7), have already been reported in other settings (Fiłoc
452 et al., 2018). At the earlier stages of PBO studies a single PBO was recognised with possible precursor
453 events (Björck et al 1997), chronologically coinciding with the presumed PBO-11.5 and PBO-11.4
454 reported here. However, these occur when CC7 growth rate is rapidly increasing (Fig. 2), which is at
455 odds with the documented growth rate decrease for PBO-11.1 and BO-10.3. At the same time, these
456 PBO-11.5 and PBO-11.4 are instead coinciding with - at times moderate - climate deterioration
457 reported above from Central Europe and Northern Spain centred at ca. 11.4 ka.
458 The scenario depicted here is a Preboreal period spanning ca. 11.4 to 11.1 ka and characterized by
459 a series of brief climate events having different local impacts and expressions. This points to major
460 hydroclimate instability within the Mediterranean at a time of low temperature variability in
461 continental Europe and polar latitudes, considering that PBO-11.1 (and BO-10.3) currently has no
462 counterpart in the higher latitudes.
463
464 **5.5. Early Holocene climate interconnections**
465 There is no generally accepted theory explaining PBO/BO events, therefore the climate mechanisms
466 producing the detected reduction of rainfall at the study site are uncertain. Ice-sheet meltwater
467 fluxes, changes in ocean ventilation and a decline in solar activity have been proposed as possible
468 forcing factors (e.g. Björk et al., 1997, 2001; Bond et al., 2001; Teller et al., 2002; van der Plicht et
469 al., 2004; Magny et al., 2007). Massive meltwater discharge events capable of decreasing the
470 formation of the North Atlantic Deep Water, as the one from glacial Lake Agassiz into the Arctic
471 Ocean via the Mackenzie River, has been invoked as the main trigger (Fisher et al. 2002). Multiple
472 events of different magnitude occurred between ca. 11.20 ka and ca. 8.2 ka (fig. 8) (Teller et al.,
473 2002) and thus procuring instabilities in the Atlantic Ocean that in turn is the main moisture source
474 for Corchia Cave according to back-trajectories reconstructions (Fig. 1) and consideration in
475 paragraph 5.2. We also notice that the d-excess in Greenland, a proxy for conditions at the moisture
476 source North Atlantic region, has an evident increase at PBO and BO times (Fig. 9). Indeed the NEEM
477 high resolution record (Gkinis et al., 2021) points to ca. 1 ‰ d-excess abrupt increment from 11.5
478 to 11.3 ka, and a similar event is centred at 10.35 ka and lasting for ca. 100 years (Fig. 9). Although
479 with a lower resolution, a d-excess rise of ca. 0.6‰ is also visible in the GRIP record (Masson-
480 Delmotte et al., 2005a) centred at 10.3 ka, while there are no apparent fluctuations during PBO
481 times. This suggests meltwater discharge impacted the climate conditions at the source in terms of

temperature, shifts in atmospheric circulation causing a relocation of the source itself, moisture uptake seasonality, atmosphere humidity and wind conditions (Steffensen et al., 2008). We can thus envision general climate instabilities within the North Atlantic due to meltwater discharge events that influenced the rainfall source for Corchia too, by either altering the SST and/or other local parameters as well as moving southward the Intertropical Convergence Zone (ITCZ) (Steffensen et al., 2008). These source-site instabilities might have triggered reduced rainfall at Corchia during PBO-11.1 and BO-10.3. However, it is important to note that the increase of several Mid-European lake-levels (Fig. 8) point to wetter conditions during the same times especially in the zone between 58º and 43º N (Magny et al., 2004; 2007). If so, the detected relative aridity within the Mediterranean cannot be related only to a general reduction of moisture availability at the source, but rather to a differential moisture distribution between the Mediterranean and European landmasses. In line with previous interpretations (Magny et al., 2004; 2007), this pattern suggests rising cyclonic activity in the mid-latitudes due to the southward shift of the Atlantic Westerly Jet and a sharper thermal gradient between high and low northern latitudes.

While our data convincingly point to a reduction of rainfall during the PBO/BOs around the western Mediterranean area, it might be difficult to constrain whether the dryness had an annual (e.g. average year-round rainfall decrease) or a seasonal (e.g. acute rainfall decrease during a few months) origin. A reduction of spring-summer rainfall is consistent with greater evaporation of lake water and reduced lake levels, as observed at Lago dell'Accesa, which is corroborated by higher charcoal levels likely reflecting increased biomass burning during longer summer droughts. Additionally, the carbonate concretions used for reconstructing the lake level are formed in the warm season, mainly corresponding to a summer signal (Magny et al., 2007). In Corchia, the isotopic composition of waters infiltrating the long-residence-time karst system (Piccini et al., 2008) is governed by the rainfall amount, but modulated by the ratio of cold/warm months precipitation and by the prevailing seasonal source of storms. A reduction of spring-summer rainfall would decrease the amount-weighted annual $\delta^{18}O$ of the infiltrating water, because of the lack of supply of high $\delta^{18}O$ rainfall from the warm seasons due to the temperature effect (Longinelli et al. 2006). Besides, the Apuan Alps receives most of its recharge during cooler months (Natali et al., 2022), thus the Preboreal-Boreal climate instability must have affected this season too. Thus, we relate the centennial-scale increase of CC7 $\delta^{18}O$ during the detected PBO/BO to a net annual reduction of rainfall sourced from the North Atlantic and potentially increased Mediterranean-sourced moisture, with the same mechanisms – although of lesser extent – operating during deglacial times.

514 Mediterranean cyclogenesis from, for example, the Gulf of Genoa, generates intense precipitation
515 events. If these were succeeded by relative dryness, this would contemporaneously: 1) reduce the
516 annual rainfall amount at Corchia; and 2) favour more evaporation at the Lago dell'Accesa in either
517 season.
518 Pollen records could potentially provide important information on PBO/BOs dynamics, but
519 convincing evidence from paleoecological archives across the Italian peninsula has been elusive
520 (Sadori and Narcisi, 2001; Allen et al., 2002). In Monticchio in southern Italy (Allen et al., 2002), the
521 PBO-11.1 is possibly occurring in a period characterized by high pollen variability (Fig. 7), while the
522 BO-10.3 is not clearly evident. This suggests insufficient attention regarding the identification of
523 these events or, as already documented in Swiss lakes (Lotter et al. 1992), the Preboreal-Boreal
524 climatic changes in certain locations did not significantly affect local vegetation. However, at Lago
525 dell'Accesa, where pollen data has a sufficiently high resolution (Drescher-Schneider et al., 2006),
526 there is evidence for a climatic deterioration possibly linked to the PBO-11.1. Faveretto et al. (2008)
527 reported evidence of Preoboreal/Boreal climatic oscillations occurring at ca 11.2 ka, 10.8–10.4 and
528 10 ka from a low-resolution pollen record from the southern Adriatic Sea. Although the age model
529 of this deep-sea core lacks the robustness of CC7, and is based on radiocarbon dating, which suffers
530 from many pitfalls in a semiclosed-basin like the Mediterranean (Siani et al., 2001; Lowe et al., 2007),
531 this study suggests that future investigations of paleoecological archives around the Mediterranean
532 may reveal the important impacts of this climatic deterioration.
533 Sea-surface temperatures obtained in cores BS79-38 and MD95-2043 from the central and western
534 Mediterranean, respectively, suggest the presence of short-lived cold events during the beginning
535 of the Holocene (Cacho et al., 2001; Sbaffi et al., 2001; Martrat et al., 2014). While the resolution of
536 the former is too poor for proposing correlations, the latter shows clear peaks in decreasing sea-
537 surface temperature between ca 11 and 9 ka, which might be the counterparts of the oscillations
538 detected in CC7, at least for BO-10.3.
539 Altogether, these data point to the impact of PBO/BOs across the Mediterranean area. Some
540 archives seem to fail in their detection either for lack of resolution or lack of *ad hoc* investigations.
541 Moreover, some proxies might not be sensitive to PBO/BOs, possibly because of the limited extent
542 of these climate fluctuations and/or because the impact might have been differential through space,
543 as occurs for other time periods (Alley et al., 2005). More local climate reconstructions will be the
544 key, in the future, for advancing our knowledge regarding the Early Holocene climate variations.
545

6. Conclusions

This paper adds further evidence of the influence of northern high-latitude climate variability in driving rainfall changes within the western Mediterranean area. This is demonstrated during both the large-scale warming at the end of the last deglaciation, as well as the lower intensity climate instabilities during the early Holocene known as Preboreal and Boreal oscillations. The $\delta^{18}O$-$\delta^{13}C$ from the CC7 stalagmite detect a substantial increase of rainfall amount reaching Corchia Cave occurring from $11.91^{+0.10}/_{-0.11}$ to $11.33^{+0.07}/_{-0.07}$, during the deglacial transition from the Younger Dryas to the Holocene. The rapid increase of stalagmite growth centred at $11.54^{+0.10}/_{-0.09}$ ka supports this interpretation. The CC7-$\delta^{18}O$ and growth rate also point to reduced rainfall during relatively short periods of the Early Holocene centered at $11.11^{+0.09}/_{-0.11}$ and $10.28^{+0.27}/_{-0.20}$ ka and correlated to PBO-11.1 and BO-10.3. These events of drier conditions are well correlated with the lake levels at Lago dell'Accesa, 150 km south of Corchia Cave, demonstrating that the reduced rainfall impacted the whole of central western Italy at centennial and intra-centennial timescale. The impact of PBO/BOs is found in several rainfall indicators throughout the western Mediterranean, highlighting that considerable changes in Mediterranean rainfall dynamics take place even during subtle instabilities at northern/Polar high latitudes. Although controversial, the occurrence of PBO/BOs has been connected to northern ice sheet meltwater fluxes within the overall deglacial warming, able to procure aridity within the western Mediterranean while central-western Europe experienced relative higher humidity.

The Earth is facing a warmer stage of the Holocene due to the current climate crisis. Climate instabilities will increase as occurred in previous warmer-than-present interglacials (Tzedakis et al., 2018). Limited extent temperature instabilities and glacial collapses at northern latitudes might thus trigger variations in rainfall dynamics within the highly populated Mediterranean area, which is already experiencing an increasing frequency of hydro-climate extremes.

Acknowledgments

This research was supported by funding from the Australian Research Council (Discovery Project number DP160102969), awarded to RD, GZ, and J. Woodhead; We are grateful to the Gruppo Speleologico Lucchese and the Federazione Speleologica Toscana for outstanding support and the Corchia Park and Parco delle Apuane authorities for the authorization supports. Thanks to three anonymous reviewers for their insightful comments.

578 **References**

579

580 Affolter, S., Häuselmann, A., Fleitmann, D., Edwards, R.L., Cheng, H. and Leuenberger, M., 2019.
581 Central Europe temperature constrained by speleothem fluid inclusion water isotopes over the past
582 14,000 years. Science Advances 5(6), 3809.

583

584 Allen, J.R.M., Brandt, U., Brauer, A., Hubbertens, H.W., Huntley, B., Keller, J., Kraml, M., Meckensen,
585 A., Mingram, J., Negendank, J.F.W., Nowaczyk, N.R., Oberhansli, H., Watts, W.A., Wulf, S., Zolitschka,
586 B., 1999. Rapid environmental changes in southern Europe during the last glacial period. Science
587 400, 740-743.

588

589 Allen, J.R.M., Watts, W.A., McGee, E., Huntley, B., 2002. Holocene environmental variability – the
590 record from Lago Grande di Monticchio, Italy. Quaternary International, 88, 69-80.

591

592 Alley, R. B., & Ágústsdóttir, A. M. (2005). The 8k event: cause and consequences of a major Holocene
593 abrupt climate change. Quaternary Science Reviews, 24(10-11), 1123-1149.

594

595 Belli, R., Frisia, S., Borsato, A., Drysdale, R.N., Hellstrom, J., Zhao, J.X., Spotl, C., (2013). Regional
596 climate variability and ecosystem responses to the last deglaciation in the northern hemisphere
597 from stable isotope data and calcite fabrics in two northern Adriatic stalagmites. Quaternary Science
598 Reviews, 72, 146e158.

599

600 Badertscher, S., Fleitmann, D., Cheng, H., Edwards, R. L., Göktürk, O. M., Zumbühl, A., Leuenberger,
601 M., Tüysüz, O. (2011). Pleistocene water intrusions from the Mediterranean and Caspian seas into
602 the Black Sea. Nature Geoscience, 4(4), 236-239.

603

604 Bajo, P., Hellstrom, J., Frisia, S., Drysdale, R., Black, J., Woodhead, J., Borsato, A., Zanchetta, G.,
605 Malcom, W., Regattieri, E., Haese, R. (2016). “Cryptic” diagenesis and its implications for speleothem
606 geochronologies. Quaternary Science Reviews, 148, 17-28.

607

608 Bajo, P., Borsato, A., Drysdale, R., Hua, Q., Frisia, S., Zanchetta, G., Hellstrom, J., Woodhead, J.
609 (2017). Stalagmite carbon isotopes and dead carbon proportion (DCP) in a near-closed-system

situation: An interplay between sulphuric and carbonic acid dissolution. Geochimica et Cosmochimica Acta, 210, 208-227.

Bajo, P., Drysdale, R. N., Woodhead, J. D., Hellstrom, J. C., Hodell, D., Ferretti, P., Voelker, A., Zanchetta, G., Rodrigues, T., Wolff, E., Tyler, J., Frisia, S., Spotl, C., Fallick, A. E. (2020). Persistent influence of obliquity on ice age terminations since the Middle Pleistocene transition. Science, 367(6483), 1235-1239.

Barker, S., Knorr, G., Edwards, R. L., Parrenin, F., Putnam, A. E., Skinner, L. C., Wolff, E., Ziegler, M. (2011). 800,000 years of abrupt climate variability. Science, 334(6054), 347-351.

Bernal-Wormull, J. L., Moreno, A., Pérez-Mejías, C., Bartolomé, M., Aranburu, A., Arriolabengoa, M., Iriarte, E., Cacho, I., Spötl, C., Edwards, R., Cheng, H. (2021). Immediate temperature response in northern Iberia to last deglacial changes in the North Atlantic. Geology, 49(8), 999-1003.

Björck, S., Kromer, B., Johnsen, S., Bennike, O., Hammarlund, D., Lehmdahl, G., Possnert, G., Rasmussen, T.L., Wohlfarth, B., Hammer, C.U., Spurk, M., 1996. Synchronized terrestrial–atmospheric deglacial records around the North Atlantic. Science 274, 1155–1160.

Björck, S., Rundgren, M., Ingòlfsson, O., Funder, S., 1997. The Preboreal oscillation around the Nordic seas: terrestrial and lacustrine responses. Journal of Quaternary Science 12, 455–465.

Björk, S., Kromer, B., Andersen, C.S., Heinemeier, J., Johnsen, S.J., Conley, D., Koc, N., Spurk, M., Veski, S., 2001. High-resolution analyses of an early Holocene climate event may imply decreased solar forcing as an important climate trigger. Geology 29, 1107-1110.

Bond, G., Kromer, R., Beer, J., Muscheler, R., Evans, M.N., Showers, W., Hoffman, S., Lotti-Bond, R., Hajdas, I., Bonani, G., 2001. Persistent Solar influence on North Atlantic Climate During the Holocene. Science, 294, 2130-2136.

Breitenbach, S.F., Plessen, B., Waltgenbach, S., Tjallingii, R., Leonhardt, J., Jochum, K.P., Meyer, H., Goswami, B., Marwan, N. and Scholz, D. (2019). Holocene interaction of maritime and continental

642 climate in Central Europe: New speleothem evidence from Central Germany. Global and Planetary
643 Change 176, 144-161.
644
645 Brunetti, M., Buffoni, L., Mangianti, F., Maugeri, M., Nanni, T. 2004. Temperature, precipitation and
646 extreme events during the last century in Italy. Global Planetary Change 40, 141–149.
647
648 Buizert, C., Gkinis, V., Severinghaus, J. P., He, F., Lecavalier, B. S., Kindler, P., Leuenberger, M.,
649 Carlson, A., Vinther, B., Masson-Delmotte, V., White, J., Liu, Z., Otto-Bliesner, B., Brook, E. 2014.
650 Greenland temperature response to climate forcing during the last deglaciation. Science, 345(6201),
651 1177-1180.
652
653 Buizert, C., Keisling, B. A., Box, J. E., He, F., Carlson, A. E., Sinclair, G., DeConto, R. M. 2018.
654 Greenland-wide seasonal temperatures during the last deglaciation. Geophysical Research Letters,
655 45(4), 1905-1914.
656
657 Cacho, I., Grimalt, J.O., Canals, M., Sbaffi, L., Shackleton, N.J., Schönfeld, J., Zahn, R., 2001. Variability
658 of the western Mediterranean Sea surface temperature during the last 25,000 years and its
659 connection with the Northern Hemisphere climatic changes. Paleoceanography, 16, 40-52.
660
661 Celle-Jeanton, H., Travi, Y., Blavoux, B., 2004. Isotopic typology of the precipitation in the Western
662 Mediterranean region at three different time scales. Geophysical Research Letters 28, 1215–1218.
663
664 Columbu, A., Chiarini, V., Spötl, C., Benazzi, S., Hellstrom, J., Cheng, H., De Waele, J. (2020).
665 Speleothem record attests to stable environmental conditions during Neanderthal–modern human
666 turnover in southern Italy. Nature ecology & evolution, 4(9), 1188-1195.
667
668 Columbu, A., Spötl, C., Fohlmeister, J., Hu, H. M., Chiarini, V., Hellstrom, J., Cheng, H., Shen, C., De
669 Waele, J. (2022). Central Mediterranean rainfall varied with high northern latitude temperatures
670 during the last deglaciation. Communications Earth & Environment, 3(1), 181.
671
672 Columbu, A., Pérez-Mejías, C., Regattieri, E., Lugli, F., Dong, X., Depalmas, A., Melis, R., Cipriani, A.,
673 Cheng, H., Zanchetta, G. and De Waele, J., (2024). Speleothems uncover Late Holocene

environmental changes across the Nuragic period in Sardinia (Italy): A possible human influence on land use during bronze to post-Iron Age cultural shifts. Quaternary Science Reviews 328, 108534.

Dalton, A. S., Margold, M., Stokes, C. R., Tarasov, L., Dyke, A. S., Adams, R. S., Allard, S., Arends, H., Atkinson, N., Attig, J., Barnett, P., Batterson, M., Bernatchez, P., Borns, H., Breckenridge, A., Briner, J., Brouard, E., Campbell, J., Carlson, A., Wright, H. (2020) An updated radiocarbon-based ice margin chronology for the last deglaciation of the North American Ice Sheet Complex. Quaternary Science Reviews, 234, 106223.

Day CC, Henderson GM (2011) Oxygen isotopes in calcite grown under cave-analogue conditions. Geochimica et Cosmochimica Acta 75: 3956–3972.

Dorale JA, and Liu ZB (2009) Limitations of Hendy test criteria in judging the paleoclimatic suitability of speleothems and the need for replication. Journal Cave Karst Studies 71: 73–80.

Drysdale, R.N., Zanchetta, G., Hellstrom, J.C., Fallick, A.E., Zhao, J-x., Isola, I., Bruschi, G., (2004). Palaeoclimatic implications of the growth history and stable isotope ($\delta^{18}O$ and $\delta^{13}C$) geochemistry of a Middle to Late Pleistocene stalagmite from central-western Italy. Earth and Planetary Science Letters 227, 215-229.

Drysdale, R.N., Zanchetta, G., Hellstrom, J.C., Fallick, A.E., Zaho J., (2005). Stalagmite evidence for the onset of the Last Interglacial in southern Europe at 129±1 ka. Geophysical Research Letters, 32, L24708

Drysdale, R.N., Hellstrom, J.C., Zanchetta, G., Fallick, A.E., Sánchez-Goni, M.F., Couchoud, I., McDonald, J., Mass, R., Lohmann, G., Isola, I. (2009). Evidence for obliquity forcing of glacial Termination II. Science, 325, 1527-1531.

Drysdale, R., Couchoud, I., Zanchetta, G., Isola, I., Regattieri, E., Hellstrom, J., Govin, A., Tzedakis, P.C., Ireland, T., Corrick, E., Greig, A., Wong, H., Piccini, L., Holden, P., Woodhead, J. (2020). Magnesium in subaqueous speleothems as a potential palaeotemperature proxy. Nature Communications, 11(1), 5027.

706

707 Masson-Delmotte, V., Jouzel, J., Landais, A., Stievenard, M., Johnsen, S. J., White, J. W. C., Wermer,
708 M., Sveinbjornsdottir, A., Fuhrer, K. (2005a). GRIP deuterium excess reveals rapid and orbital-scale
709 changes in Greenland moisture origin. Science, 309(5731), 118-121.
710
711 Masson-Delmotte, V., Landais, A., Stievenard, M., Cattani, O., Falourd, S., Jouzel, J., Fischer, H.
712 (2005b). Holocene climatic changes in Greenland: Different deuterium excess signals at Greenland
713 Ice Core Project (GRIP) and NorthGRIP. Journal of Geophysical Research: Atmospheres, 110(D14).
714
715 Fiłoc, M., Kupryjanowicz, M., Rzodkiewicz, M., Suchora, M., 2018. Response of terrestrial and lake
716 environments in NE Poland to Preboreal cold oscillations (PBO). Quaternary International, 475, 101-
717 117.
718
719 Fink, A. H., Brücher, T., Krüger, A., Leckebusch, G. C., Pinto, J. G., Ulbrich, U. (2004). The 2003
720 European summer heatwaves and drought-synoptic diagnosis and impacts. Weather, 59(8), 209-
721 216.
722
723 Fisher, T.G., Smith, D.G., Andrews, J.T., 2002. Preboreal oscillation caused by a glacial Lake Agassiz
724 flood. Quaternary Science Reviews 21, 873–878.
725
726 Fohlmeister, J. (2012a). A statistical approach to construct composite climate records of dated
727 archives. Quaternary Geochronology, 14, 48-56.
728
729 Fohlmeister, J., Schröder-Ritzrau, A., Scholz, D., Spötl, C., Riechelmann, D.F., Mudelsee, M.,
730 Wackerbarth, A., Gerdes, A., Riechelmann, S., Immenhauser, A. and Richter, D.K., (2012b). Bunker
731 Cave stalagmites: an archive for central European Holocene climate variability. Climate of the Past
732 8, 1751-1764.
733
734 Fohlmeister, J., Voarintsoa, N. R. G., Lechleitner, F. A., Boyd, M., Brandtstätter, S., Jacobson, M. J.,
735 Oster, J. L. (2020). Main controls on the stable carbon isotope composition of speleothems.
736 Geochimica et Cosmochimica Acta, 279, 67-87.
737

738 Fohlmeister, J., Sekhon, N., Columbu, A., Vettoretti, G., Weitzel, N., Rehfeld, K., Veiga-Pires, C., Ben-
739 Yami, M., Marwan, N. and Boers, N., (2023). Global reorganization of atmospheric circulation during
740 Dansgaard–Oeschger cycles. Proceedings of the National Academy of Sciences 120(36),
741 p.e2302283120.
742
743 Frisia, S., Borsato, A., Fairchild, I., McDermott, F. (2000). Calcite fabrics, growth mechanisms, and
744 environments of formation in speleothems from the Italian Alps and southwestern Ireland. Journal
745 of Sedimentary Petrology 70, 1183–1196.
746
747 García-Alix, A., Camuera, J., Ramos-Román, M. J., Toney, J. L., Sachse, D., Schefuß, E., Yanes, Y.
748 (2021). Paleohydrological dynamics in the Western Mediterranean during the last glacial cycle.
749 Global and Planetary Change, 202, 103527.
750
751 Giorgi, F. (206) Climate change hot-spots. Geophys. Res. Lett. 33, L08707.
752
753 Grant, K. M., Rohling, E. J., Bar-Matthews, M., Ayalon, A., Medina-Elizalde, M., Ramsey, C. B., Satow,
754 C., Roberts, A. P. (2012). Rapid coupling between ice volume and polar temperature over the past
755 150,000 years. Nature, 491(7426), 744-747.
756
757 Hellstrom, J.C., 2003. Rapid and accurate U/Th dating using parallel ion-counting multi-collector ICP-
758 MS. Journal of Analytical Atomic Spectrometry 18, 135-136.
759
760 Hellstrom, J.C., 2006. U–Th dating of speleothems with high initial ^{230}Th using stratigraphical
761 constraint. Quaternary Geochronology 1, 289-295.
762
763 Hendy CH (1971) The isotopic geochemistry of speleothems – I. The calculation of the effect of
764 different modes of formation on the isotopic composition of speleothems and their applicability as
765 palaeoclimatic indicators. Geochimica et Cosmochimica Acta 219: 807– 824.
766
767 Hodell, D., Crowhurst, S., Skinner, L., Tzedakis, P. C., Margari, V., Channell, J. E., Kamenov, G.,
768 Maclachlan, S., Rothwell, G. 2013. Response of Iberian Margin sediments to orbital and suborbital
769 forcing over the past 420 ka. Paleoceanography, 28(1), 185-199.

Hoek, W.Z., Bos J.A.A., 2007. Early Holocene climate oscillations – causes and consequences. Quaternary Science Reviews, 26, 1901-1906.

Ionita M., Tallaksen L.M., Kingstone D.G., Stagg J.H., Laaha G., Van Lanen H.A., Scholz P., Chelcea S.M., Haslinger K., 2017. The European 2015 drought from a climatological perspective Hydrol. Earth Syst. Sci., 21, 1397–1419.

IPCC working group (2023). Climate Change 2023: Synthesis Report. Contribution of Working Groups I, II and III to the Sixth Assessment Report of the Intergovernmental Panel on Climate Change.

Isola, I., Ribolini, A., Zanchetta, G., Bini, M., Regattieri, E., Drysdale, R. N., Hellstrom, J., Bajo, P., Montagna, P., Pons-Branchu, E. (2019a). Speleothem U/Th age constraints for the Last Glacial conditions in the Apuan Alps, northwestern Italy. Palaeogeography, Palaeoclimatology, Palaeoecology, 518, 62-71.

Isola, I., Zanchetta, G., Drysdale, R. N., Regattieri, E., Bini, M., Bajo, P., Hellstrom, J., Baneschi, I., Lionello, P., Woodhead, J., Greig, A. (2019b). The 4.2 ka event in the central Mediterranean: new data from a Corchia speleothem (Apuan Alps, central Italy). Climate of the Past, 15(1), 135-151.

Lechleitner, F. A., Amirnezhad-Mozhdehi, S., Columbu, A., Comas-Bru, L., Labuhn, I., Pérez-Mejías, C., Rehfeld, K. (2018). The potential of speleothems from Western Europe as recorders of regional climate: a critical assessment of the SISAL database. Quaternary, 1(3), 30.

Longinelli, A., Anglesio, E., Flora, O., Iacumin, P., Selmo, E., (2006). Isotopic composition of precipitation in Northern Italy: reverse effect of anomalous climatic events. Journal of Hydrology 329, 471-476.

Lotter, A.F., Eicher, U., Siegenthaler, U., Birks, H.J.B. 1992. Late-glacial climate oscillations as recorded in Swiss lake sediments. Journal of Quaternary Science, 7, 187-204.

802 Lowe, J.J., Blockley, S., Trincardi, F., Asioli, A., Cattaneo, A., Matthews, I.P., Pollard, M., Wulf, S. 2007:
803 Age modelling of late Quaternary marine sequences in the Adriatic: Towards improved precision
804 and accuracy using volcanic event stratigraphy. Continental Shelf Research 27, 560-582.
805
806 Luppichini M., Bini M., Barsanti M., Giannecchini R., Zanchetta G. 2022. Seasonal rainfall trends of
807 a key Mediterranean area in relation to large-scale atmospheric circulation: How does current
808 global change affect the rainfall regime? Journal of Hydrology 612, 128233.
809
810 Magny M., Marguet A., Chassepot G. H., Billaud Y. 2001. Early and late Holocene water-level
811 fluctuations of Lake Annecy, France: sediment and pollen evidence and climatic implications.
812 Journal of Paleolimnology, 25(2), 215-227.
813
814 Magny M., Bégeot C. 2004. Hydrological changes in the European midlatitudes associated with
815 freshwater outbursts from Lake Agassiz during the Younger Dryas event and the early Holocene.
816 Quaternary Research 61, 181-192.
817
818 Magny, M., Vannière, B., de Beaulieu, J-L., Bégeot, C., Heiri, O., Millet, L., Peyron, O. and Walter-
819 Simonnet, A-V. 2007: Early-Holocene climatic oscillations recorded by lake-level fluctuations in
820 west-central Europe and in central Italy. Quaternary Science Reviews, 26, 1951–1964.
821
822 Martrat, B., Jimenez-Amat, P., Zahn, R., and Grimalt, J.O., 2014, Similarities and dissimilarities
823 between the last two deglaciations and interglaciations in the North Atlantic region. Quaternary
824 Science Reviews, 99, 122–134
825
826 McDermott, F. (2004). Palaeo-climate reconstruction from stable isotope variations in speleothems:
827 a review. Quaternary Science Reviews, 23(7-8), 901-918.
828
829 Mühlinghaus C, Scholz D, Mangini A (2009) Modelling fractionation of stable isotopes in stalagmites.
830 Geochimica et Cosmochimica Acta 73: 7275-7289.
831

Muschitiello, F., D'Andrea, W. J., Schmittner, A., Heaton, T. J., Balascio, N. L., DeRoberts, N., Caffee, M., Woodruff, T., Welten, K., Skinner, L., Simon, M., Dokken, T. (2019). Deep-water circulation changes lead North Atlantic climate during deglaciation. Nature Communications, 10(1), 1272.

Natali, S., Baneschi, I., Doveri, M., Giannecchini, R., Selmo, E., Zanchetta, G. (2021). Meteorological and geographical control on stable isotopic signature of precipitation in a western Mediterranean area (Tuscany, Italy): Disentangling a complex signal. Journal of Hydrology, 603, 126944.

Natali, S., Doveri, M., Giannecchini, R., Baneschi, I., Zanchetta, G. (2022). Is the deuterium excess in precipitation a reliable tracer of moisture sources and water resources fate in the western Mediterranean? New insights from Apuan Alps (Italy). Journal of Hydrology, 614, 128497.

Natali, S., Doveri, M., Franceschi, L., Giannecchini, R., Luppichini, M., Menichini, M., Zanchetta, G. (2023). Moisture sources and climatic effects controlling precipitation stable isotope composition in a western Mediterranean island (Pianosa, Italy). Atmospheric Research, 294, 106987.

North Greenland Ice Core Project (NGRIP) Members. High-resolution record of Northern Hemisphere climate extending into the last interglacial period. Nature 431, 147–151 (2004).

Osman, M. B., Tierney, J. E., Zhu, J., Tardif, R., Hakim, G. J., King, J., & Poulsen, C. J. (2021). Globally resolved surface temperatures since the Last Glacial Maximum. Nature 599, 239-244.

Piccini, L., Zanchetta, G., Drysdale, R.N., Hellstrom, J.; Isola, I., Fallick, A.E., Leone, G., Doveri, M., Mussi, M., Mantelli, F., Molli, G., Lotti, L., Roncioni, A., Regattieri, E., Meccheri, M., Vaselli, L., (2008). The environmental features of the Monte Corchia cave system (Apuan Alps, central Italy) and their effects on speleothem growth. International Journal of Speleology 37, 153-173

Rasmussen, S.O., Bigler, M., Blockley, S.P., Blunier, T., Buchardt, S.L., Clausen, H.B., Cvijanovic, I., Dahl-Jensen, D., Johnsen, S.J., Fischer, H., Gkinis, V., Guillevic, M., Hoek, W.Z., Lowe, J.J., Pedro, J.B., Popp,T., Seierstad, I.K., Steffensen, J.P., Svensson, A.M., Vallelonga, P., Vinther, B.M., Walker, M.J.C., Wheatley, J.J., Winstrup, M. (2014). A stratigraphic framework for abrupt climatic changes during

the Last Glacial period based on three synchronized Greenland ice-core records: refining and extending the INTIMATE event stratigraphy. Quaternary Science Reviews, 106, 14-28.

Regattieri, E., Querci, S., Zanchetta, G., Zanella, E., Isola, I., Drysdale, R. N., Hellstrom, J, Magrì, F. (2021). Interstadial conditions over the Southern Alps during the early penultimate glacial (MIS 6): a multiproxy record from Rio Martino Cave (Italy). Quaternary Science Reviews, 257, 106856.

Rolph, G., Stein, A., Stunder, B., 2017. Real-time Environmental applications and Display sYstem: READY. Environmental Model. Software 95, 210–228.

Sadori, L., Narcisi, B., 2001. The Postglacial record of environmental history from Lago di Pergusa. The Holocene 11, 655-670.

Sbaffi, L., Wezel, F.C., Kallel, N., Paterne, M., Cacho, I., Pivieri, P., Shackleton, N., 2001. Response of the pelagic environment to paleoclimatic changes in the central Mediterranean during the Late Quaternary. Marine Geology, 178, 39-62.

Siani, G., Magny, M., Paterne, M., Debret, M., Fontugne, M. (2013) Paleohydrology reconstruction and Holocene climate variability in the South Adriatic Sea. Climate of the Past 9, 499–515.

Siani, G., Paterne, M., Michel, E., Sulpizio, R., Sbrana, A., Arnold, M., Haddad, G., 2001. Mediterranean sea surface radiocarbon reservoir age changes since the Last Glacial Maximum. Science 294, 1917-1920.

Skinner, L. C., Fallon, S., Waelbroeck, C., Michel, E., Barker, S. Ventilation of the deep Southern Ocean and deglacial CO_2 rise. Science 328, 1147–1151 (2010).

Steffensen, J. P., Andersen, K. K., Bigler, M., Clausen, H. B., Dahl-Jensen, D., Fischer, H., White, J. W. (2008). High-resolution Greenland ice core data show abrupt climate change happens in few years. Science, 321(5889), 680-684.

Stein, A.F., Draxler, R.R., Rolph, G.D., Stunder, B.J.B., Cohen, M.D., Ngan, F., 2015. NOAA's HYSPLIT Atmospheric Transport and Dispersion Modeling System. Bulletin of the American Meteorological Society 96, 2059–2077.

Surić, M., Columbu, A., Lončarić, R., Bajo, P., Bočić, N., Lončar, N., Drysdale, R.N. and Hellstrom, J.C., 2021. Holocene hydroclimate changes in continental Croatia recorded in speleothem δ13C and δ18O from Nova Grgosova Cave. The Holocene 31(9), 1401-1416.

Teller, J.T., Leverington, D.W., Mann, J.D., 2002. Freshwater outbursts to the oceans from Lake Agassiz and their role in climate change during the last deglaciation. Quaternary Science Reviews 21, 879–887.

Toucanne, S., Minto'o, C. M. A., Fontanier, C., Bassetti, M. A., Jorry, S. J., Jouet, G. (2015). Tracking rainfall in the northern Mediterranean borderlands during sapropel deposition. Quaternary Science Reviews, 129, 178-195.

Treble, P. C., Baker, A., Abram, N. J., Hellstrom, J. C., Crawford, J., Gagan, M. K., Borsato, A., Griffiths, A., Bajo, P., Markowska, M., Priestley, S., Hankin, S., Paterson, D., 2022. Ubiquitous karst hydrological control on speleothem oxygen isotope variability in a global study. Communications Earth & Environment, 3(1), 29

Tremaine, D. M., Froelich, P. N., Wang, Y. (2011) Speleothem calcite farmed in situ: modern calibration of $\delta^{18}O$ and $\delta^{13}C$ paleoclimate proxies in a continuously-monitored natural cave system. Geochimica et Cosmochimica Acta 75, 4929–4950.

Tzedakis, P. C., Drysdale, R. N., Margari, V., Skinner, L. C., Menviel, L., Rhodes, R. H., Taschetto, A.S., Hodell, D.A., Crowhurst, S.J., Hellstrom, J.C., Fallick, A.E., Grimalt, J. O., McManus, J. F., Martrat, B., Mokeddem, Z., Parrenin, F., Roe, K., Zanchetta, G. (2018). Enhanced climate instability in the North Atlantic and southern Europe during the Last Interglacial. Nature communications, 9(1), 4235.

van der Plicht, J., van Geel, B., Bohncke, S.J.P., Bos, J.A.A., Blaauw, M., Speranza, A.O.M., Muscheler, R., Björck, S., 2004. The Preboreal climate reversal and a subsequent solar forced climate shift. Journal of Quaternary Science 19, 263–269.

Vannière, B., Colombaroli, D., Chapron, E., Leroux, A., Tinner, W., Magny, M., 2008. Climate versus human-driven fire regimes in Mediterranean landscapes: the Holocene record of Lago dell'Accesa (Tuscany, Italy). Quaternary Science Reviews, 27(11-12), 1181-1196.

von Grafenstein, U., Erlenkeuser, H., Brauer, A., Jouzel, J., Johnsen, S. J. A mid-European decadal isotope-climate record from 15,500 to 5000 years BP. Science 284, 1654–1657 (1999).

Warner, M.S.C., 2018. Introduction to PySPLIT: a Python Toolkit for NOAA ARL's HYSPLIT Model. Computing in Science & Engineering 20, 47–62.

Zanchetta, G., Drysdale, R. N., Hellstrom, J. C., Fallick, A. E., Isola, I., Gagan, M. K., Pareschi, M. T. (2007). Enhanced rainfall in the Western Mediterranean during deposition of sapropel S1: stalagmite evidence from Corchia cave (Central Italy). Quaternary Science Reviews, 26(3-4), 279-286.

Zanchetta G., Baneschi I., Magny M., Sadori L., Termine R., Bini M., Vanniere B., Desmet M., Natali S., Luppichini M., Pasquetti F., 2022. Insight into summer drought in southern Italy: palaeohydrological evolution of Lake Pergusa (Sicily) in the last 6700 years. Journal of Quaternary Science, 37, 1280-1293.

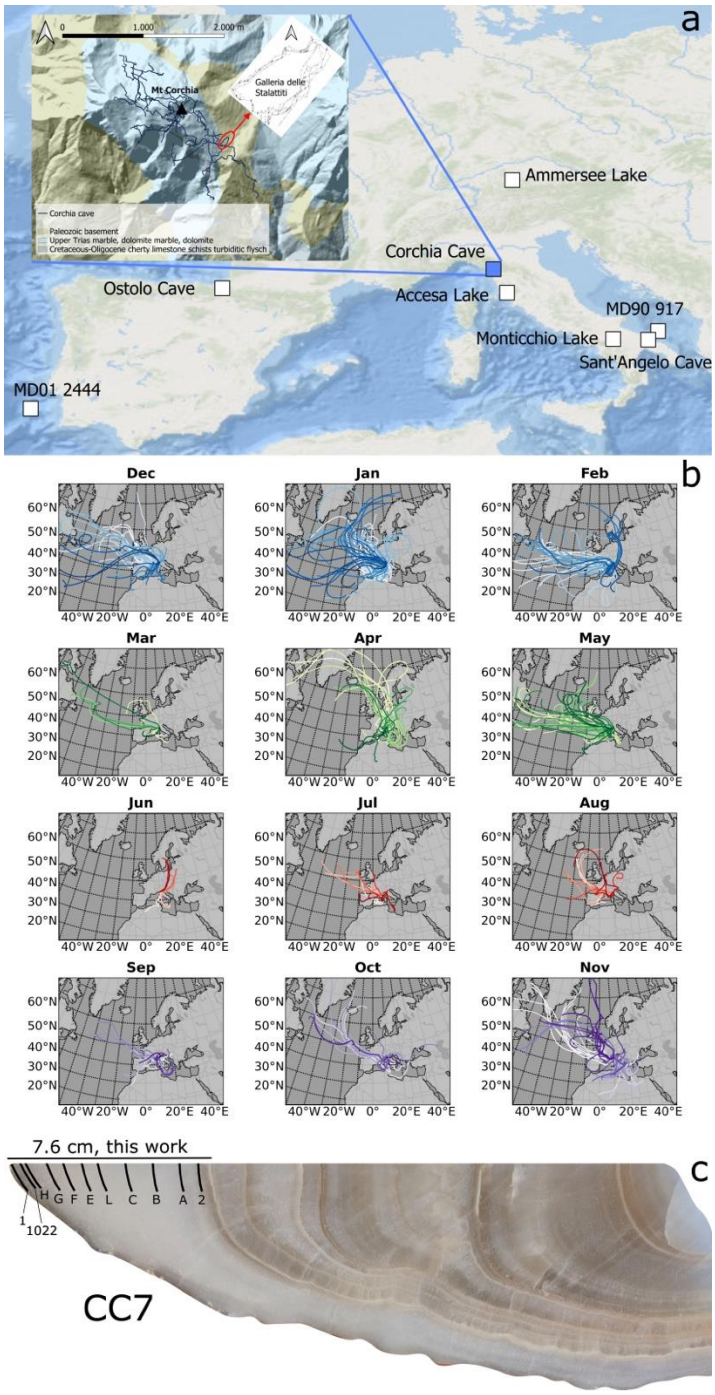

Figure 1. Study area. A general map reporting the location of Corchia Cave and the other circummediterranean records used for comparison. The small inlet shows the extension and planimetry of Corchia Cave, within the geological context. Below, the CC7 stalagmite. Only the first 7,6 cm from the top have been considered for this work. The locations of U-Th dates are reported with black bars and IDs, while the $\delta^{18}O$-$\delta^{13}C$ analyses, at ca 200 µm spacing, have been constructed along the stalagmite growth axis.

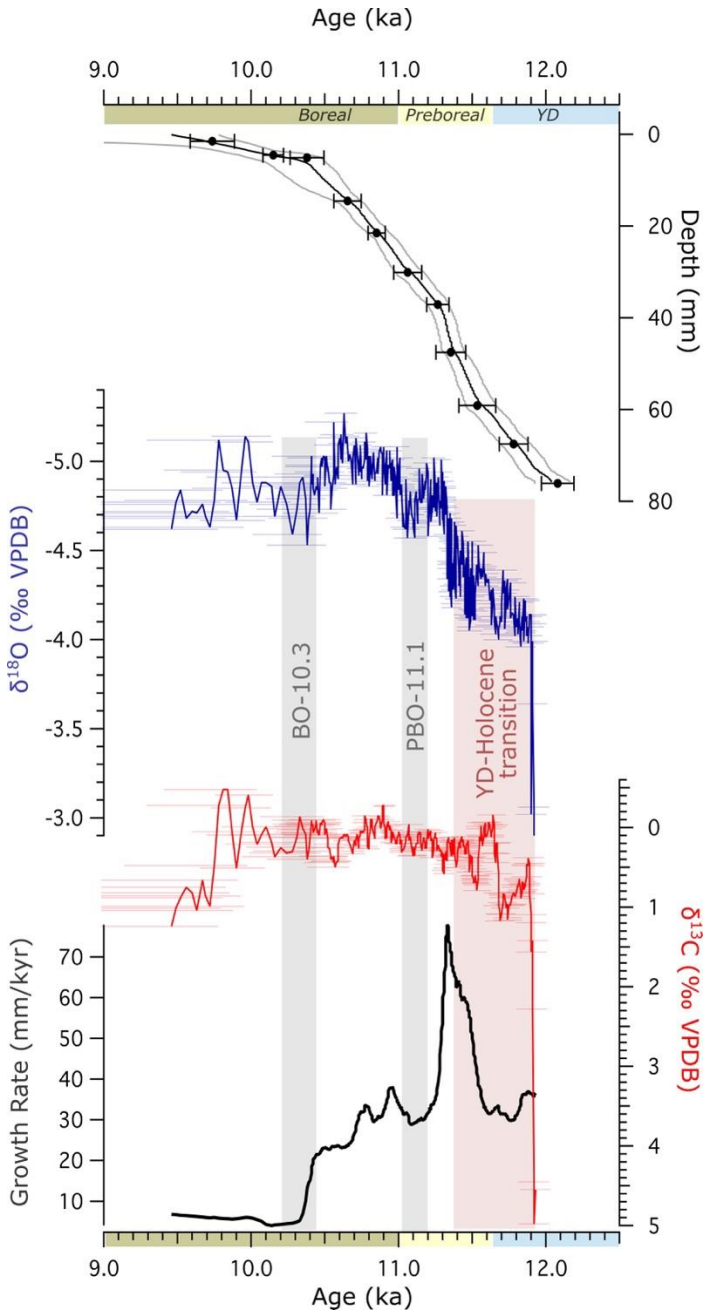

Figure 2. CC7 timeseries. From top to bottom: CC7 age model, $\delta^{18}O$ and $\delta^{13}C$ timeseries with blue and red line respectively, and growth rate. $\delta^{18}O$-$\delta^{13}C$ curves report chronological uncertainty bars. Vertical red and grey shadows highlight the climate episode discussed in this paper: the deglacial transition and the preboreal oscillations (PBO/BO) at 11.1 and 10.3 ka. The x-axis reports the Younger Dryas (YD) and preboreal chronozones.

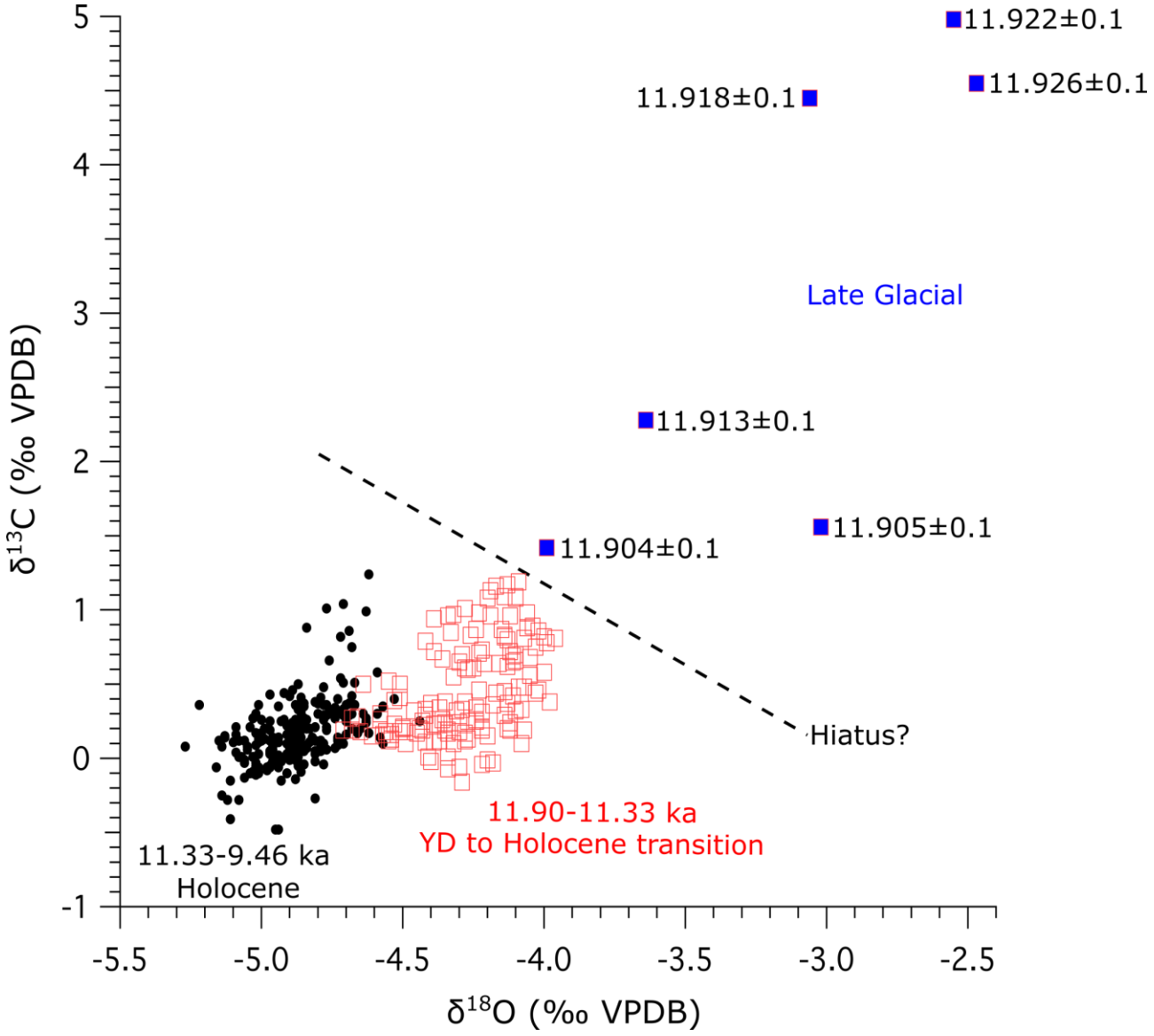

Figure 3. CC7 $\delta^{18}O$-$\delta^{13}C$. Results of $\delta^{18}O$-$\delta^{13}C$ in CC7 form three main clusters, associated with the Younger Dryas (YD) chronozone (blue squares and ages), deglacial transition (red squares) and Holocene (black dots). The presence of a hiatus is supposed, although it cannot be constrained by the age model.

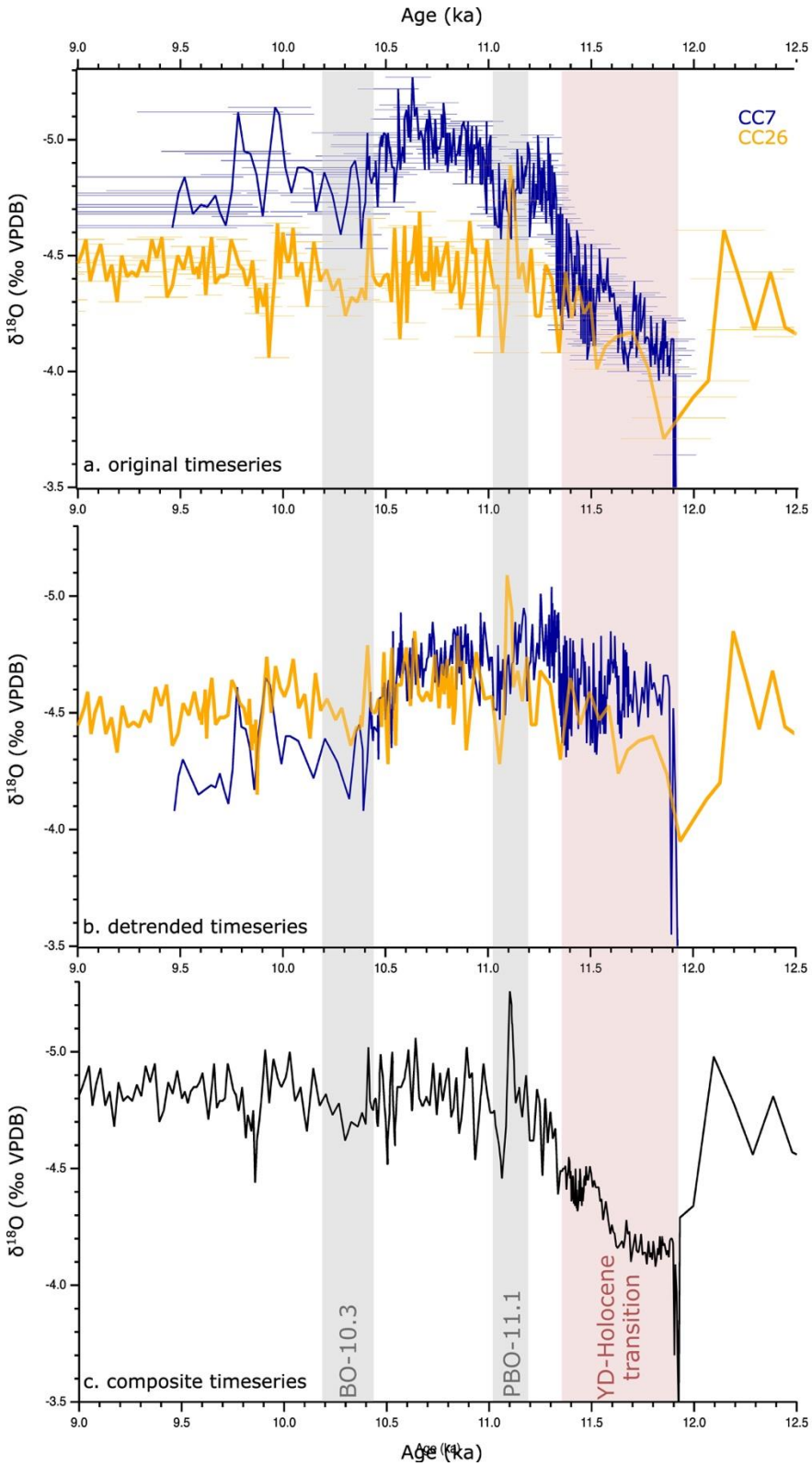

Figure 4. The replication test. a) Plotted with their own original chronologies, CC7 $\delta^{18}O$ (blue) is compared to CC26 (orange, Zanchetta et al., 2007; Bajo et al., 2017). The two curves appear similar, within age uncertainties (error bars). b) the two curves are detrended by using iscam (Fohlmeister, 2012). Note that iscam recalculates the age-depth model with a different approach with respect the one used for the original chronologies, so small discrepancies can occur. c) the composite CC7-CC26 record calculated by iscam. See text for details. Colored shadows are the same as Fig. 2.

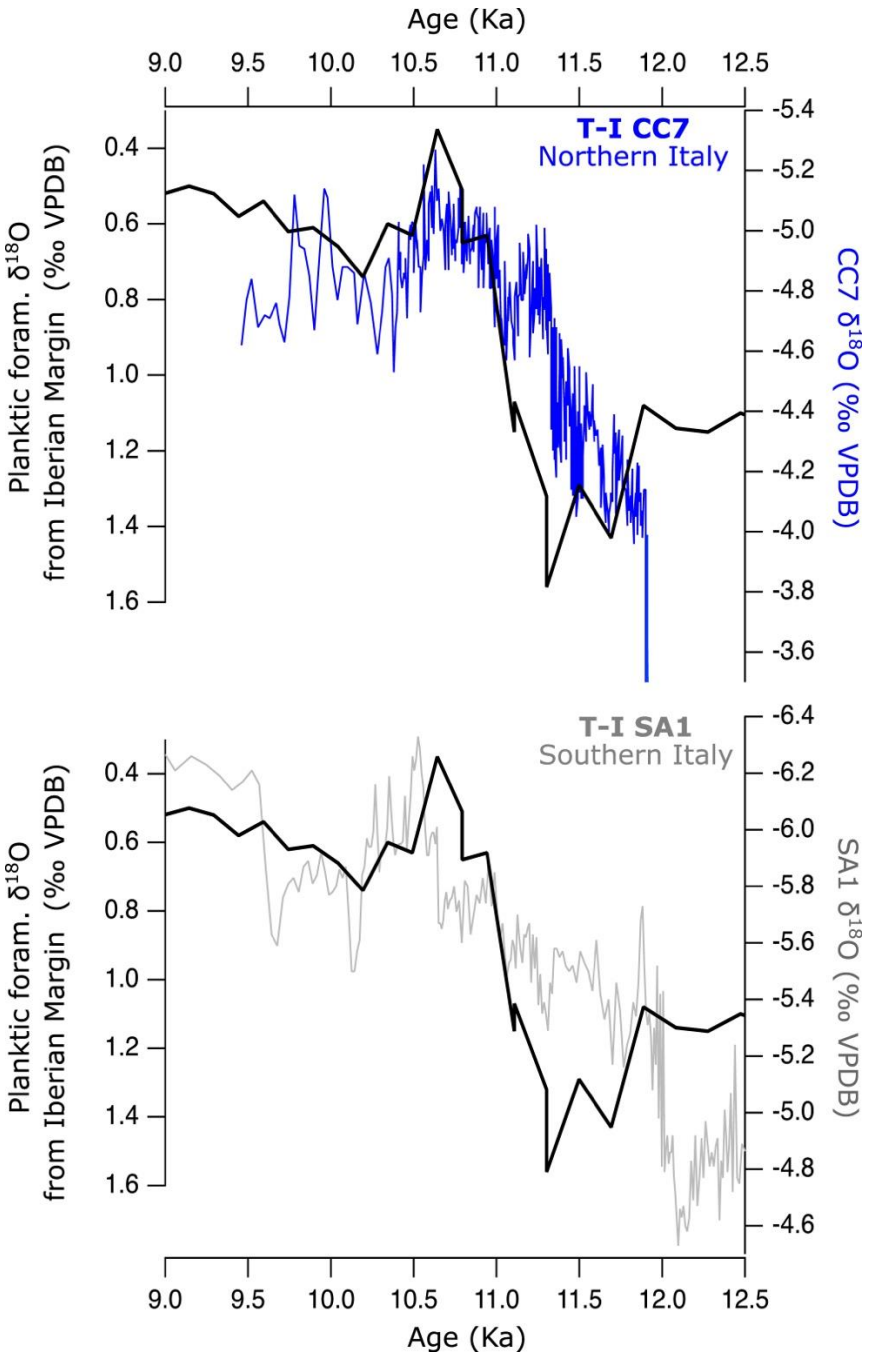

Figure 5. Deglacial conditions in the Mediterranean and Iberian margin. YD to Holocene patterns of $\delta^{18}O$ from a speleothem from the north (CC7, upper panel, this study) and south (SA1, lower panel, Columbu et al., 2022) are compared to $\delta^{18}O$ from planktic foraminifera from the Iberian Atlantic margin (Hodell et al., 2013). All records are plotted against their own chronologies.

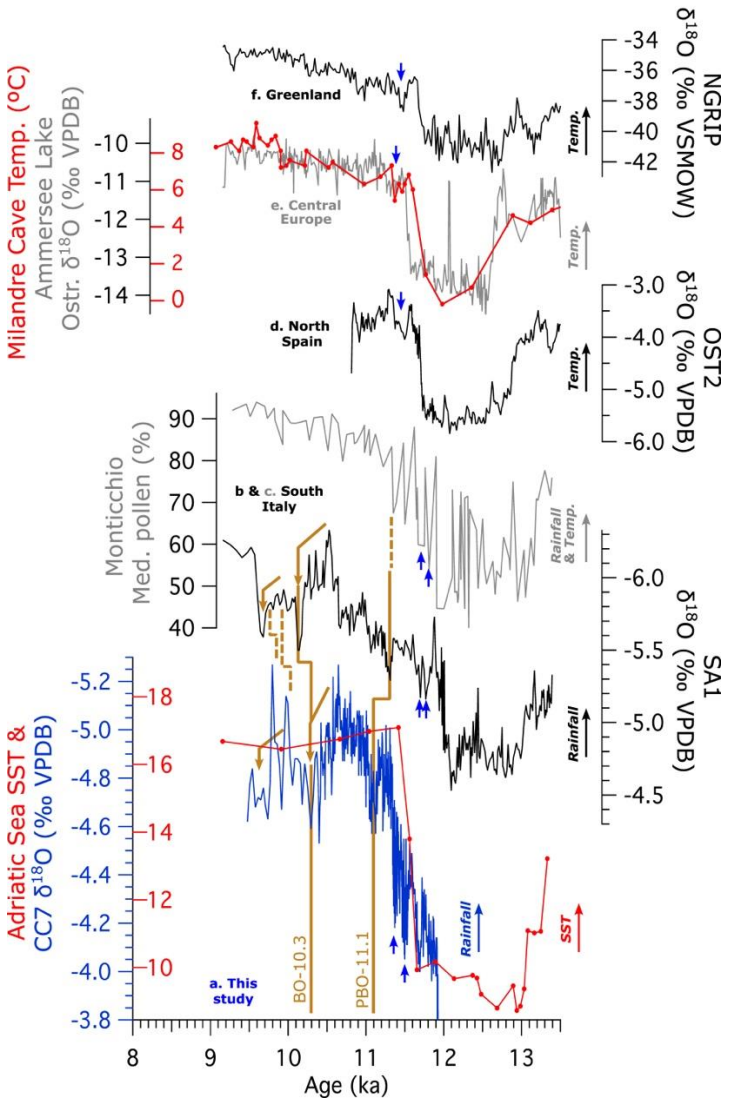

Figure 6. CC7 compared with regional and local records. a) CC7 $\delta^{18}O$ (blue line, this study) and Adriatic SST (red line, Siani et al., 2013); b) SA1 speleothem $\delta^{18}O$ from Sant'Angelo Cave in southern Italy (Columbu et al., 2022); c) Mediterranean pollen from Lago Grande di Monticchio Lake southern Italy (Allenn et al., 1999); d) OST2 speleothem $\delta^{18}O$ from Ostolo Cave in northern Spain (Bernal-Wormull et al., 2021); e) Ostracods $\delta^{18}O$ from Ammersee Lake in central Germany (grey line, von Grafenstein et al., 1999) and paleotemperature reconstruction from Milandre Cave, respectively in northwestern Switzerland (red line, Affolter et al., 2019); f) Ice core $\delta^{18}O$ from Greenland (NGRIP, 2004). Arrows on the right side indicate the climate interpretation for each record. Vertical brown bars highlights the PBO-11.1 across and BO-10.3 in CC7 and SA1 speleothems recors. Brown arrows indicate the similar pattern of $\delta^{18}O$ variability of these latter pre, during and post BO-10.3. Blue small arrows indicate the presumed forerunner PBO-11.5 and PBO-11.4 in Italian records as well as the climate deterioration at around 11.4 ka at higher latitudes (see text for details).

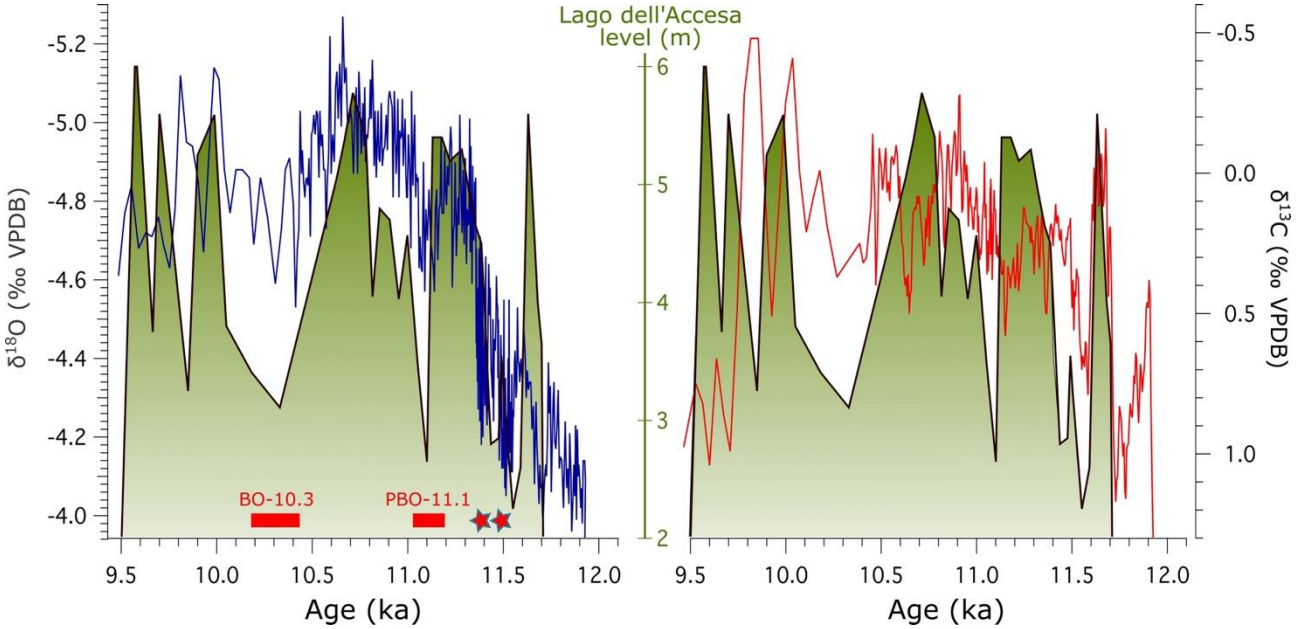

Figure 7. CC7 vs Lago dell'Accesa lacustrine record. CC7 $\delta^{18}O$ (blue line, on the left) CC7 $\delta^{13}C$ (red line, on the right) are compared to the variation of the Lago dell'Accesa level (green line and shadows, on the background) (Magny et al., 2007). The events discussed in the text (BO-10.3 and PBO-11.1, red bars) are better constrained in CC7 $\delta^{18}O$ than $\delta^{13}C$. Red stars instead indicate the presumed forerunner PBO-11.5 and PBO-11.4 (see text for details).

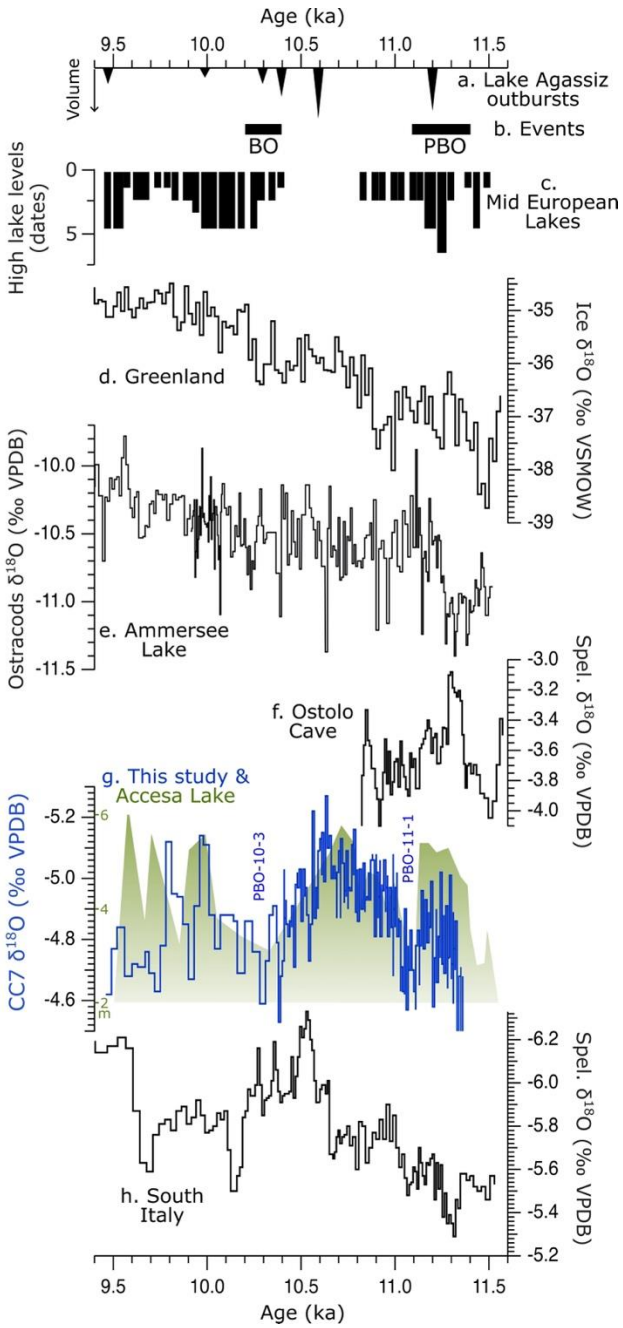

Figure 8. CC7 and focus on regional Early Holocene records. a) Timing and relative volumetric magnitude of Lake Agassiz outbursts (Teller et al., 2002); b) timespan of PBO and BO according with Björk et al., 1996, 1997, and 2001; c) number of dates indicating high levels of mid-European lakes (Magny et al., 2004; 2007); d) ice core $\delta^{18}O$ from Greenland (NGRIP, 2004); e) Ostracods $\delta^{18}O$ from Ammersee Lake in central Germany (von Grafenstein et al., 1999); f) OST2 speleothem $\delta^{18}O$ from Ostolo Cave in northern Spain (Bernal-Wormull et al., 2021); g) CC7 $\delta^{18}O$ (blue line, this study) and Lago dell'Accesa level (green shadows on the background, Magny et al., 2007); h) SA1 speleothem $\delta^{18}O$ from Sant'Angelo Cave in southern Italy (Columbu et al., 2022)

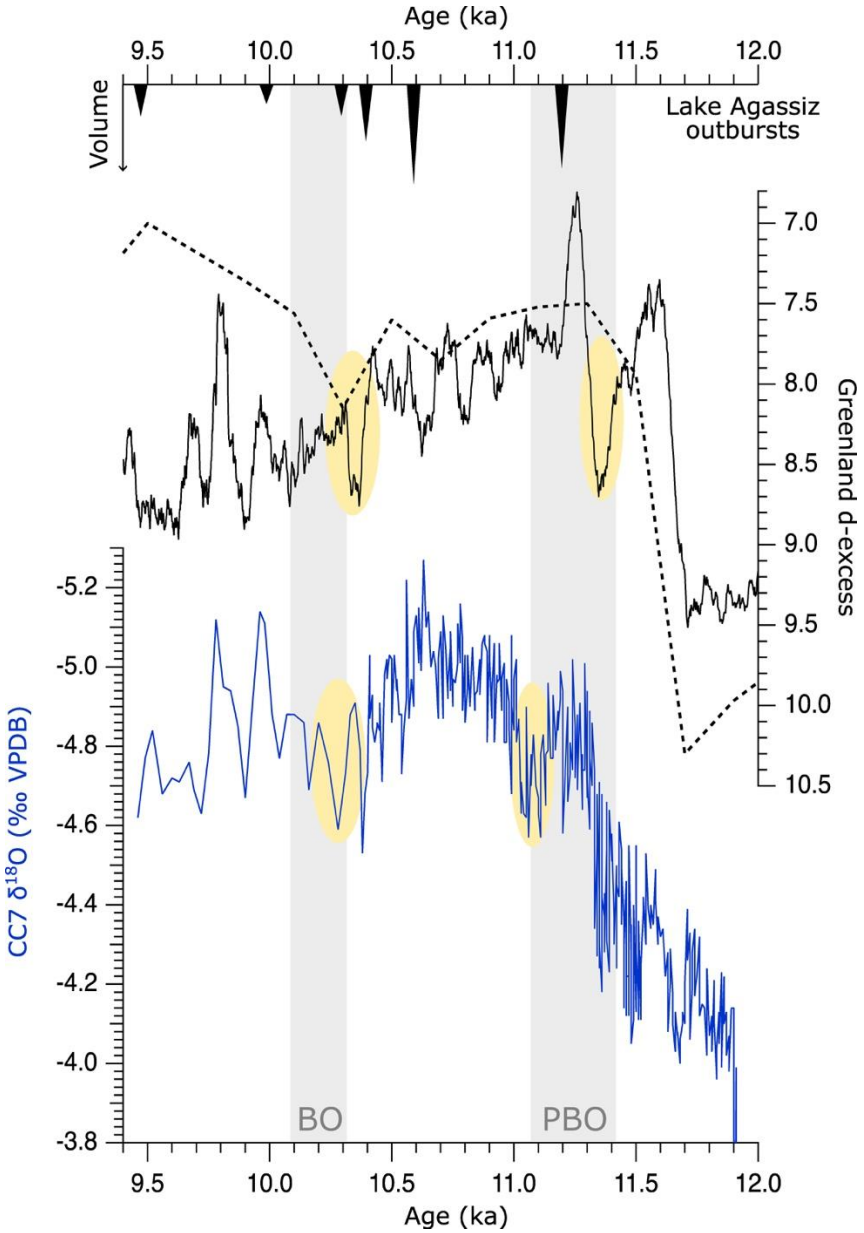

Figure 9. CC7 vs GRIP d-excess record. CC7 $\delta^{18}O$ (blue line) compared to Greenland GRIP (dotted line, Masson-Delmotte et al., 2005a) and NEEM record (full line, Gkinis et al., 2021) d-excess, which is a proxy for changes in the source site procuring moisture for Greenland. Lake Agassiz uotbursts (black arrows, Teller et al., 2002) and the timing of PBO/BO (gray shadows, Björk et al., 1996; 1997; 2001) are given, together with the expression of PBO/BO in CC7 and Greenland d-excess (yellow shadows).

Sample	Mass (mg)	Depth (mm)	$^{230}Th/^{238}U_A \pm 2\sigma$	$^{234}U/^{238}U_A \pm 2\sigma$	Uncorrected age ± 2σ (ka)	$^{230}Th/^{232}Th_A$	Corrected age ± 2σ (ka)	Corrected $[^{234}U/^{238}U_A]_{initial} \pm 2\sigma$
CC7-1	4.4	1.5	0.0572 ± 0.0009	0.6723 ± 0.0016	9.736 ± 0.151	/	**9.731 ± 0.157**	0.6632 ± 0.0017
CC7 1022	9.3	4.5	0.0594 ± 0.0004	0.6717 ± 0.0012	10.150 ± 0.074	/	**10.146 ± 0.078**	0.6622 ± 0.0013
CC7-H	/	5.1	0.0610 ± 0.0006	0.6725 ± 0.0025	10.448 ± 0.116	6715.8	**10.379 ± 0.115**	0.6627 ± 0.0026
CC7-G	/	14.5	0.0622 ± 0.0005	0.6692 ± 0.0012	10.722 ± 0.094	13173.5	**10.654 ± 0.093**	0.6590 ± 0.0013
CC7-F	/	21.5	0.0634 ± 0.0003	0.6705 ± 0.0012	10.918 ± 0.059	7643.3	**10.851 ± 0.059**	0.6602 ± 0.0013
CC7-E	/	30.1	0.0645 ± 0.0005	0.6700 ± 0.0015	11.128 ± 0.095	8657.5	**11.062 ± 0.095**	0.6595 ± 0.0016
CC7-L	/	37.1	0.0660 ± 0.0004	0.6719 ± 0.0013	11.368 ± 0.077	1625.8	**11.293 ± 0.077**	0.6612 ± 0.0014
CC7-C	/	47.5	0.0663 ± 0.0005	0.6711 ± 0.0017	11.437 ± 0.097	918.3	**11.355 ± 0.101**	0.6603 ± 0.0018
CC7-B	/	59.1	0.0675 ± 0.0006	0.6718 ± 0.0017	11.644 ± 0.115	370.1	**11.535 ± 0.125**	0.6609 ± 0.0018
CC7-A	/	67.5	0.0688 ± 0.0005	0.6732 ± 0.0016	11.857 ± 0.097	1535.6	**11.781 ± 0.098**	0.6621 ± 0.0017
CC7-2	4.8	76.1	0.0702 ± 0.0006	0.6737 ± 0.0015	12.080 ± 0.110	/	**12.076 ± 0.117**	0.6623 ± 0.0016

Table 1

Age data and sample depths for stalagmite CC7. The values are presented with ±2σ uncertainties. Isotope data are expressed as activity ratios. 230Th/238U is determined using a mixed spike calibrated against a solution of HU-1 - see Hellstrom (2003) for the detailed protocol. Age is calculated using the standard U–Th age equation, by decay constants of 9.195×10^{-6} and 2.835×10^{-6} for ^{230}Th and ^{234}U respectively. Corrected age is calculated allowing for an initial 230Th/232Th of 0.8 ± 0.7, included as an additional term in the standard U–Th age equation. $^{234}U/^{238}U_{initial}$ is calculated using $^{234}U/^{238}U$ and the corrected age.